**Grant Agreement Number 608553**

**IMAGE**
**Integrated Methods for Advanced Geothermal Exploration**

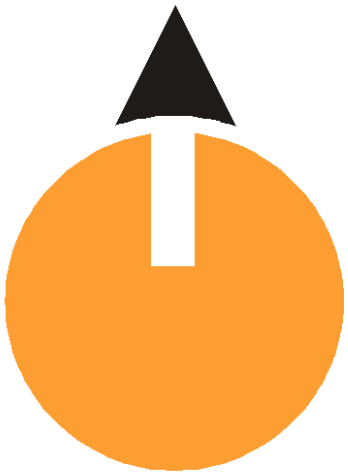

# IMAGE-D5.6:
# MT-Inversion techniques with external constraints

| | |
|---|---|
| Responsible author | Gylfi Páll Hersir (ISOR) and Adele Manzella (CNR-IGG) |
| Responsible SP-leader | Gylfi Páll Hersir (ISOR) |
| Responsible WP-leader | Adele Manzella (CNR) |
| Contributions by: | Ásdís Benediktsdóttir, Gylfi Páll Hersir, Knútur Árnason, Guðni Karl Rosenkjær, Ragna Karlsdóttir (ISOR)<br>Serena Botteghi, Enrico Calvi, Assunta Donato, Gianluca Gola, Adele Manzella, Giordano Montegrossi, Alessandro Santilano, Eugenio Trumpy, Sandra Trifirò (CNR-IGG)<br>Luigi Capozzoli, Gregory De Martino, Valeria Giampaolo, Felice Perciante, Enzo Rizzo, Gerardo Romano (CNR-IMAA)<br>Alberto Godio (CNR-IGG and Politecnico di Torino) |

# 1 Introduction and summary

This report describes *MT-inversion techniques with external constraints*, Deliverable D5.6 within the IMAGE project. *Report analysing the results of MT-inversion techniques with external contraints, describing optimal MT layout and data modelling for obtaining maximum information from MT surveys, including recommendations for opitmised MT site spacing for different a-priori constraints.*

The first part of the report, which was performed by ISOR, discusses the origin and nature of the static shifts and some tested methods for static shift correction, i.e. joint 1D inversion of co-located TEM and MT and spatial filtering and statistical assumptions about the shifts. A software is introduced which inverts the two datasets for both the resistivity model and the shift of the MT. Besides determining the static shift, joint inversion is an important quality check of the TEM and MT data sets, i.e. weather they are compatible. In EM surveying, software should be used make a preliminary joint inversion of TEM and MT at base camp as a quality control to make sure the field mission is not terminated until god quality data have been collected. Finally, the claim that 3D inversion of MT can deal with the static shifts, i.e. introduce shallow resistivity structures (not resolved by the data) to account for the shifts is tested.

The second part was done by ISOR. On one hand the depth-location of a low-resistivity anomaly, as observed from borehole data, is build into the starting model, giving the program a headstart into gaining information on the resistivity in the survey area and on the other hand information on the ductile-brittle bounday location is used to infer the location of a deep low-resistivity anomaly, which is put into the starting model of the inversion. Several tests have been done on the site spacing in MT for 3D inversion.n This was done for MT data from the Hengill area in SW-Iceland, starting with a measurment and model grid of 1 km by 1 km (see, Árnason et al., 2010). Later a measurement and model grid seize of 500 m by 500 m was tested which improved the resolution significantly for the uppermost 1 to 2 km (Árnason, pers. comm., June 2017). Finally, a measurement and model grid seize 250 m by 250 m was tested (Benediktsdóttir, pers. comm., June 2017). It only improved the resolution moderately.

In the third part performed by CNR, an integrated approach is proposed that greatly improved the knowledge on the deep structures of the system on the basis of the critical review of deep well data, geological and geophysical data and the analysis of new and previously acquired MT data in the Larderello-Travale field. Resistivity models by 2D deterministic inversion was achieved, focusing on the understanding of the reliability of the a-priori model for the inversion procedure. Three sets of starting models were implemented and tested: A homogeneous (without external constraints), a geological model (from the integrated model) and finally an interpolation of 1D models. The resulting models constrained with detailed and accurate geological information as well as using 1D models showed higher resolution than those unconstrained (i.e. from homogeneous half-space). It is demonstrated how the a-priori information from the analysis of MT data, i.e. by PSO optimization in this case, greatly improved the inversion results even those geologically constrained, which is not a trivial issue for the exploration of geothermal greenfield, due to lack of underground data.

# Table of Content

# 2 Part one: Static shift correction, joint 1D inversion of co-located TEM and MT

## 2.1 Introduction

Task 5.3 was meant to be a continuation of a previous EU-supported I-GET project and the then on-going multinational project "Advanced 3D Geophysical Imaging Technologies for Geothermal Resource Characterization" (3DIM). The aim of 3DIM was to implement the so-called „cross-gradient minimisation" to constrain resistivity models in inversion of MT data by other data sets, such as seismic tomography. The rationale for this approach was that electromagnetic fields in conductive media (the Earth) obey diffusion equations and hence loose resolution (exponentially) with distance from the source (surface). Seismic wave signals, on the other hand, obey the wave equation and should inherently have better resolution at depth.

This was a very ambitious goal, requiring merging of inversion codes for different datasets into one inversion code. It became, however, clear that to implement this approach needed much more effort than was available within the 3DIM project. Then an alternative "leap frog" approach was tried, using seismic tomography models as cross-gradient constraint in MT inversion and vice versa. This effort was undertaken by LBL in USA and Uppsala University in Sweden, using proprietary MT and seismic tomography inversion software developed at the two respective institutions and not available to the IMAGE project. The limited budget of the 3DIM did, however, not allow the effort needed to make this into an operational approach and software tool. The lesson learned from the 3DIM project was that joint/constrained inversion of different geophysical data sets is a subject needing more extensive (academic) research and code development than allowed in the 3DIM and the IMAGE projects.

The joint/constrained inversion is meant to reduce ambiguity in the inversion of MT data. 3D inversion of MT is inherently an underdetermined (ill-posed) problem because it involves much more unknowns than data values. To make the inversion stabile and meaning full the 3D resistivity models have to be regularised by some constraints, such as smoothness. The joint/constrained inversion should allow educated relaxation of the smoothing but that is complicated to implement.

There are other ambiguities involved in extracting information about the subsurface resistivity structure from MT data. These ambiguities are not due to ambiguity in the inversion process, but in the MT data themselves. This could be distortion due to cultural noise, but the most serious one is the so called static shift ambiguity caused by near surface resistivity anomalies. These anomalies affect the apparent resistivity. **The problem is that the anomalies causing the distortion are not resolved by the MT data themselves.** This means that other data are needed to constrain or correct the MT data before they are inverted. Failing to do so, can lead to seriously wrong resistivity models.

Various methods have been proposed to deal with this problem. Using co-located TEM soundings to correct for the MT static shift is commonly used. Other methods like spatial filtering and/or some statistical assumptions about the shifts have also been tried. Since 3D inversion of MT became available, some people (and service venders) claim that the inversion is capable of adjusting the shallow resistivity structure, not resolved by the MT data, to account for the shifts. This is a compelling claim, indicating that other datasets are not needed, resulting in cheaper surveying.

It was decided to devote one part of the work within Task 5.3 to further address the issue of how to deal with the static shifts in MT. The origin and nature of the static shifts is discussed and some tested methods for static shift correction, i.e. joint 1D inversion of co-located TEM and MT and spatial filtering and statistical assumptions about the shifts. The principle behind TEM method is fundamentally different from that of the MT, making the two datasets complimentary and TEM can be used as "external" constraint on the MT data. The joint inversion is done by a software, named TEMTD. The software inverts the two datasets for both the resistivity model and the shift of the MT. The development of this software started in the IGET and 3DIM projects mentioned above and was developed further under the IMAGE project to make it a versatile and powerful tool for inversion of TEM and MT data. Besides determining the static shift, joint inversion is an important quality check of the TEM and MT data sets, i.e. weather they are compatible. In EM surveying, software should be used make a preliminary joint inversion of TEM and MT at base camp as a quality control to make sure the field mission is not terminated until god quality data have been collected. Furthermore, it is described how the TEMTD software is used to correct for static shifts of MT prior to 2D and 3D inversion. Finally, the claim that 3D inversion of MT can deal with the static shifts, i.e. introduce shallow resistivity structures (not resolved by the data) to account for the shifts is tested.

## 2.2 The static shift problem of MT

The MT method, like all resistivity methods that is based on measuring the electric field in the surface, suffer the so-called telluric or static shift problem manifesting itself in an unknown multiplier of the apparent resistivity (a constant shift on log-scale). This phenomenon is caused by resistivity in-homogeneities close to the electric dipoles. Severe topography can also lead to static shifts. Except for very high frequencies, the shifts are independent frequency. Static shifts can be extreme in geothermal areas in volcanic environments where resistivity variations are often huge. The problem is made even worse by the fact that the shifts are often not random. All soundings in large contiguous areas can be consistently shifted up or down. Extreme examples of this are presented here.

It is sometimes claimed that the static shifts can be dealt with by resolving the shallow resistivity structure around the electric dipole by measuring at high enough frequencies. This would hold true if the earth can be considered as a pure Ohmic conductor. But at high frequencies other processes set in. Capacitance and induced polarization effects become important and lead to reduction of the electric field and consequently bias the apparent resistivity down at very high frequencies.

Various techniques to use the MT data themselves to identify and correct for static shifts have been proposed and tried. These "pseudo" corrections are usually based on some spatial averaging and/or some statistical assumptions about the shifts e.g. that the shift multipliers are random and that the product of the shift multipliers of individual soundings is close to one for sufficiently many soundings covering large areas. It is shown here that this assumption is far from being true in geothermal areas in volcanic environments.

Since 3D inversion of large MT datasets became available, some service vendors have claimed that the 3D inversion can cope with static shifts. By detailed modelling of topography, shifts of topographic origin can be modeled to some extent. But it has also been claimed that shifts due to shallow resistivity in-homogeneities can be dealt with by using fine model grids near the surface. The inversion would then introduce appropriate resistivity bodies at shallow depth. This has, however, not been demonstrated convincingly in the literature.

The central-loop TEM method is only sensitive to the near surface resistivity structure and topography at very early times. At late times their effects have practically disappeared. Here it is shown that a joint inversion of MT and TEM data is a consistent and effective way to correct for static shifts in MT soundings and should be used in 1D and prior to 2D and 3D inversion. If static shifts are corrected for by TEM, topography should not be modelled in the inversion; that would account twice for shifts due to topography. It is the view of the author that, except in special cases like thick and homogeneous sediments close to the surface, MT data alone should be considered as incomplete data for geothermal exploration.

The Magneto Telluric (MT) method is widely used to study the resistivity structure of the earth down to the depth of tens or even hundreds of kilometres. The MT method, like all resistivity methods that are based on measuring electric field in the surface, suffers the so-called telluric or static shift problem. The shift problem comes about because the electromagnetic field is distorted by shallow resistivity anomalies at, or close to, the sounding site and/or topography. Except at very high frequencies, the magnetic field is not much affected (Groom, 1988) but the electric field can be severely affected. At very high frequencies the electric field is distorted both by induced Eddy currents and galvanic distortion. At lower frequencies (below a few hundred Hz), most commonly used in geothermal exploration, the electric field is practically only subject to galvanic distortion and has an unknown frequency independent multiplier, relative to the undistorted field, causing shifts of the apparent resistivity curves when plotted on log-scale.
The unknown shift multiplier in the apparent resistivity directly scales the resistivity values obtained by interpretation of the soundings. According to the dependence of the depth of penetration (skin-depth) on the resistivity, depths to resistivity boundaries will be also be scaled by the square root of the multiplier. It is therefore evident that interpretation of un-corrected MT data can lead to drastically wrong resistivity models. The purpose of this paper is to review the telluric shift problem. It will be demonstrated, both by model calculations and study of field data, that the shifts can be severe, both up and down, and what is even worse, they can be systematic in large contiguous areas.

## 2.3 Shifts due to near-surface resistivity anomalies

Static shifts caused by resistivity in-homogeneities close to the electric dipoles of the MT soundings can be thought of as arising from two phenomena: 1) electric field distortion due to the dependency of the electric field (voltage gradient) on the resistivity of the material where the current is flowing and the voltage difference is measured and 2) current distortion (current channelling or repelling).

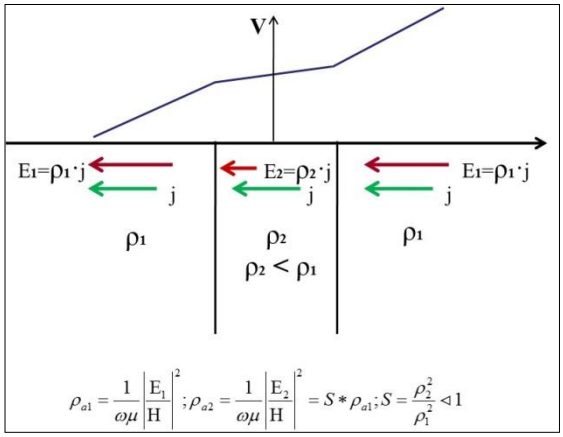


**Figure 1:** *Electric field distortion causing shift*.

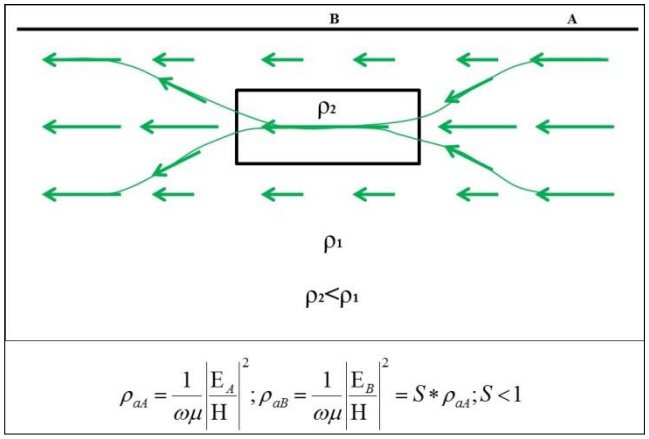


**Figure 2:** *Current distortion causing shift.*

Figure 1 shows schematically the variation of the voltage and electric field (slope of the voltage curve) in the surface when a constant current density flows through 2D domains of different resistivity (extending infinitely deep). On the figure, green arrows indicate the constant current density and the red arrows the electric field driving the current. In this example $\rho_2 < \rho_1$ and the electric field (or the voltage difference over a given length) is lower in the low resistivity domain. Unless at very high frequencies where Eddy currents may be induced, this lowering of the electric field is independent of the frequency of an alternating current. According to the definition (given in Fig. 1) the apparent resistivity will be lower in domain 2 than outside. If $\rho_2 > \rho_1$ the electric field and the apparent resistivity would be higher in the central domain than outside.

The other phenomenon, current channelling, is schematically illustrated on Figure 2. When current is flowing in the ground with a localised resistivity anomaly, the current density (green arrows) is deflected. If the anomaly is of lower resistivity than the surroundings, the current density is deflected (channelled) into the anomaly resulting in smaller surface current density and electric field and hence lower apparent resistivity at a point B above the anomaly than at a point a far away. if the resistivity is higher than the surroundings, the current is repelled out of the anomaly resulting in higher resistivity at point B than at point A. Like for the voltage distortion, this effect is independent of the frequency of the current density except at very high frequencies. The phase difference between the electric and magnetic fields, and hence apparent phase is, on the other hand not distorted except at very high frequencies and Eddy currents are induced in the anomaly.

An observant reader will note that if the surface anomaly on Figure 1 would have limited depth extend, or generally limited spatial extend, current channelling will counteract the electric field distortion to some extent, but as will be shown below, the electric field distortion will dominate.

To demonstrate how these effects affect MT soundings, simple model calculations similar to those presented by Sternberg et al. (1988) are shown here. The model calculations are done by the 3D code wsinw3dmt (Siripunvaraporn et al., 2005). Two cases are presented. Case-1 is a 3m thick 300m x 300m low resistivity surface patch of 5 Ωm in a 500 Ωm surface layer of a simple layered model (443 m of 500 Ωm, 300 m of 10 Ωm, 10 km of 50 Ωm and 10 Ωm basement). Case-2 is a 300 m x 300 m and 30 m thick 5 Ωm low resistivity body at 13m depth in the 500 Ωm top layer of the same layered model as in Case-1. For planar view and sections through the models see Figure 3.

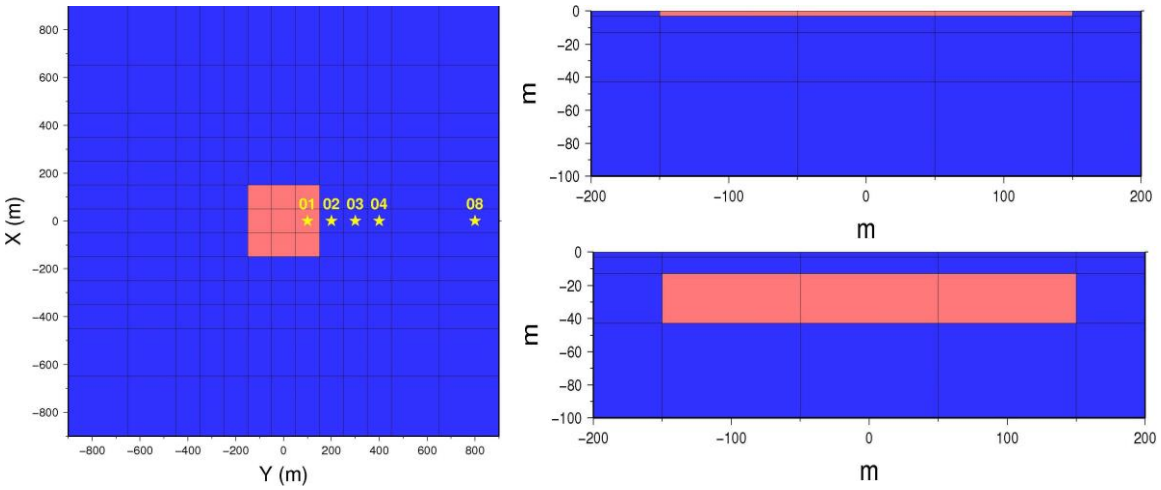


**Figure 3:** *Left, planar view of resistivity anomalies; Case-1 (surface to 3m) and Case-2 (13m to 43m). Near surface vertical section at x=0 through model in Case-1 (top right) and in Case-2 (bottom right)*

The MT response was calculated for 31 periods from $10^{-3}$ s to $10^{3}$ s, and for five stations as shown on Figure 3 (station-01 at 100m, -02 at 200m, -03 at 300m, -04 at 400m and -08 at 800m distance from the centre of the anomaly). Figure 4 shows the calculated apparent resistivity and phase for the xy (Ex/Hy, red stars) and yx (Ey/Hx, green stars) polarizations respectively for stations 01 through 04 for Case-1. For comparison, the coincident responses for the two polarizations at location 08 are shown (purple lines).

Figure 4a shows that inside the patch the apparent resistivity for both polarizations is shifted severely down by the same amount due to voltage distortion. At very high frequency (short periods), induced Eddy currents in the patch play a role and the phase deviates from that of station 08, but at periods longer than $10^{-2}$ s, the phase is practically undistorted while the apparent resistivity is scaled down (shifted on log scale) relative to that of station-08 by a multiplier practically independent of period (frequency). For station-02, 50m outside the patch (Figure 4b), current channelling causes the apparent resistivity of the xy polarization to be shifted down but the yx polarization to be shifted up. The x-component, parallel to the resistivity discontinuity, is reduced because some current is channelled away from the site and into the low resistivity while

the y-component, perpendicular to the discontinuity, is increased by the current channelling into the anomaly. The phase is a bit distorted at very short periods due to Eddy currents. Further away from the anomaly, the shifts decrease and have practically disappeared at station-08, 650m outside the anomaly.

Figure 5 shows the apparent resistivity and phase for the xy- and yx-polarization for stations 01 through 04 for Case-2. The shifts are similar to but more extreme than in Case-1 and the phase is distorted by induction effects to longer periods, especially above the conductive body. Figure 6 shows the apparent resistivity and phase calculated from the determinant of the impedance tensor for station-02 for both Cas-1 and Case-2. The figure shows that for the thin surface patch the determinant apparent resistivity is not shifted but for the berried low resistivity body it is shifted down. This is consistent with Figures 4b and 5b because apparent resistivity from the rotationally invariant determinant are in a way an “average” over all directions. The observation, that the determinant apparent resistivity is less affected by surface in-homogeneity close to the sounding site is of importance because it shows that, if TEM sounding is not available for static shift correction, inversion of the determinant apparent resistivity (or apparent resistivity derived from the average of the off-diagonal elements of the tensor) is less prone to errors than inversion of the individual polarisations.

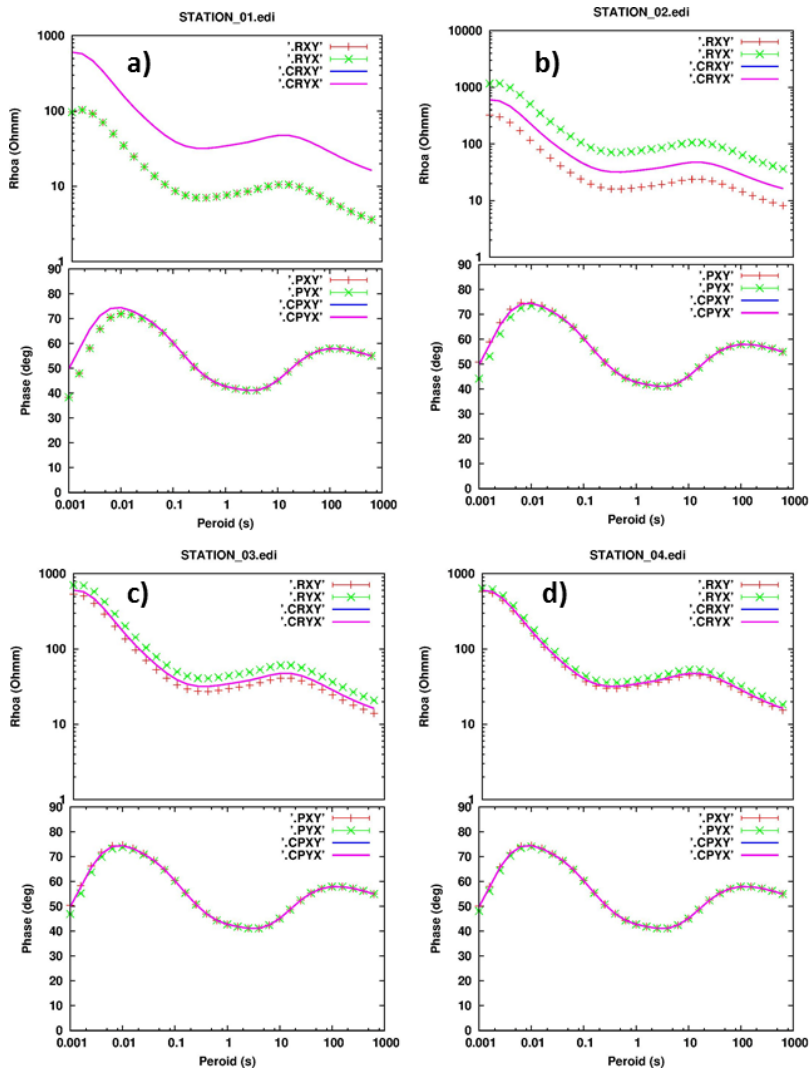


**Figure 4:** *Calculated apparent resistivity and phase for Case-1 (low resistivity surface patch) for stations 01 (a), 02 (b), 03 (c) and 04 (d). The xy and yx polarizations are shown as green and red stars, respectively. The coincident xy and yx polarizations for station 08 are shown for comparison by purple solid lines.*

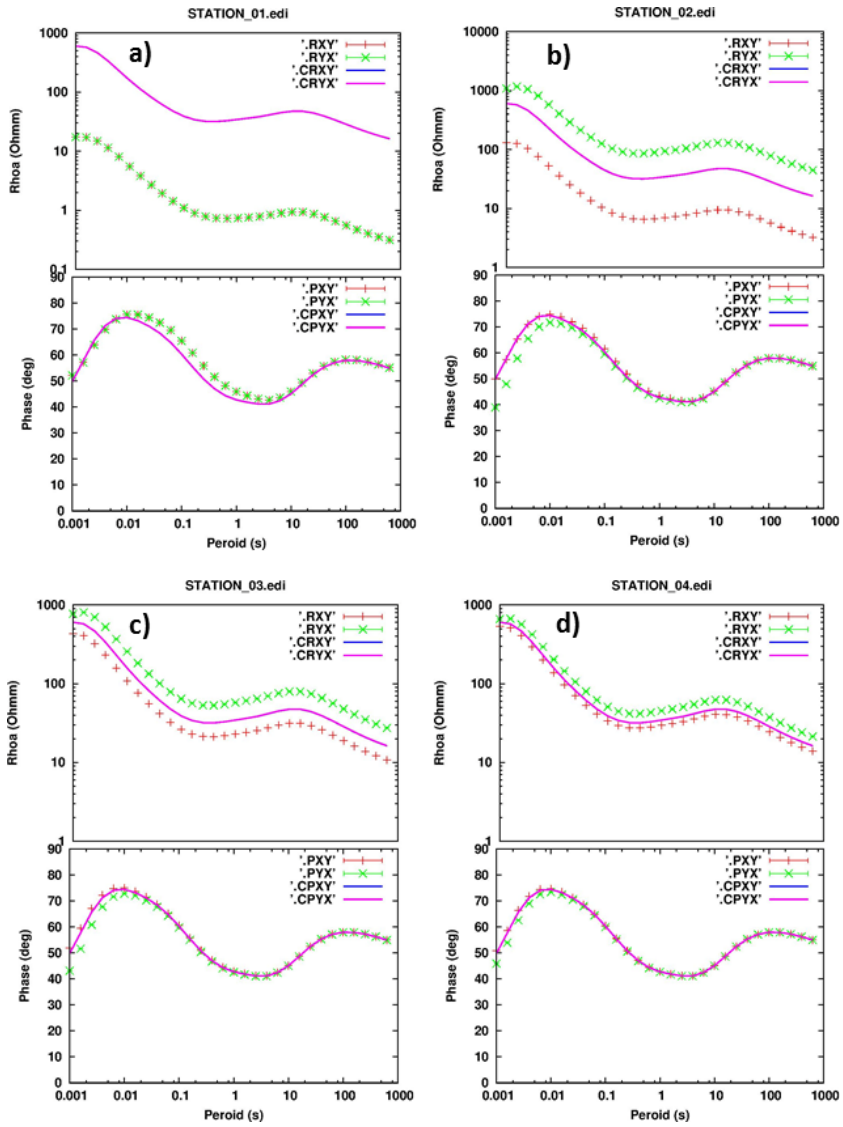


**Figure 5:** *Calculated apparent resistivity and phase for Case-2 (low resistivity body at 13m depth) for stations 01 (a), 02 (b), 03 (c) and 04 (d). The xy and yx polarizations are shown as green and red stars, respectively. The coincident xy and yx polarizations for station 08 are shown for comparison by purple solid lines.*

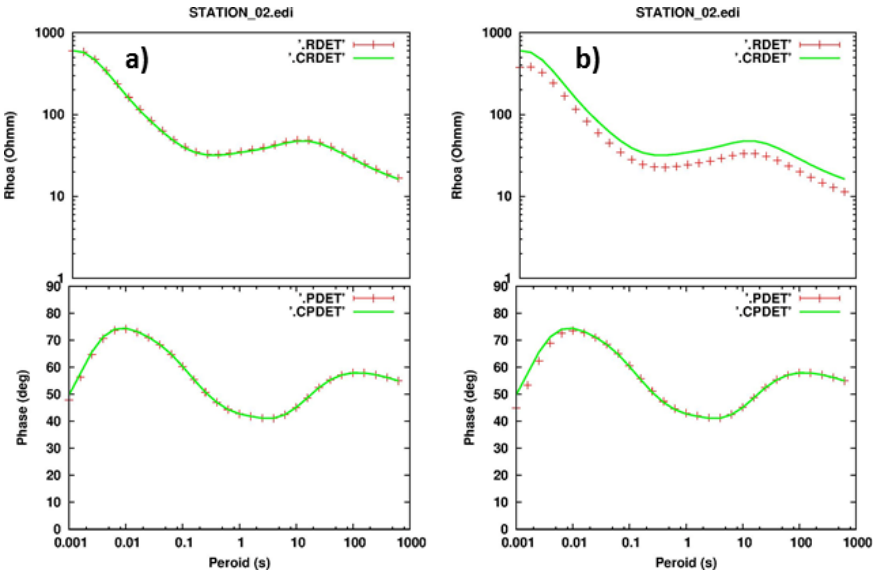


**Figure 6:** *Apparent resistivity and phase calculated from the determinant of the impedance tensor at station 02 for Case-1 (a) and Case-2 (b).*

We have seen here two examples where local resistivity anomalies close to the electric dipoles of MT soundings can result in severe shifts. Both of these circumstances are quite common in geothermal areas in volcanic environment. They are often characterised by very resistive surface lavas. Where the geothermal fluid reaches the surface there can be patches of very conductive clay alteration surrounded by very resistive lavas, producing severe voltage distortion. If the conductive clay minerals dome up to shallow depth but not quite to the surface, they can result in extensive current channelling.

## 2.4 Topographic effects

Topography can also lead to static shifts by current distortion as shown schematically on Figure 7. The induced current density, flowing mostly laterally, is spread out in local topographic highs but concentrated in topographic lows. In the case of constant resistivity earth, this will lead to apparent resistivity lower than the true resistivity on topographic highs and higher in topographic lows.

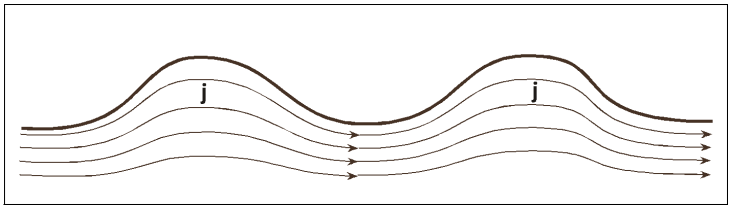


**Figure 7:** *Distortion of induced current density in homogeneous earth due to topography.*

An example of this is demonstrated on Figures 8 and 9. The data are from a joint MT and TEM survey of the Montelago geothermal prospect on the island of Mindoro in the Philippines (Hersir et al., 2014). The Montelago area has a very rugged topography characterized by very steep, 100-200 m high ridges and hills with narrow valleys in between. The Figures show static shift

multipliers of the MT apparent resistivity derived from the determinant of the tensor. The shift multipliers were determined by joint inversion with central-loop TEM soundings at the same spots (within < 50 m; for further discussion of this procedure see below). Figure 9 shows that shifts down (S < 1) are much more common than shifts up. Figure 8 shows that the spatial distribution of the shift multipliers correlates with the topography, showing soundings at high altitude more shifted down than soundings at topographic lows. This is also seen on Figure 9 where the shift multipliers are plotted versus elevation of the soundings. Even though the Figure shows considerable scattering, it is evident that in general the shift multipliers decrease with increasing elevation. It should not be concluded here that MT data are generally more shifted down at high altitudes; the correlation here is because in this case the higher altitude data are on ridges or peaks, not on plateaus, and the low altitude soundings are generally in narrow valleys.

Figure 9 is quite informative. Firstly, it shows that shifts down are much more common that shifts up (several examples showing the same are presented below). Secondly, the scatter and general decrease of the shift multiplier with elevation shows that, in the case of substantial topography, shifts are due to both in-homogeneities at the sounding site and topography. Thirdly, it was found that, even in this rather extreme topography, a joint inversion with central-loop TEM (with small source loops of 100 m x 100 m) could consistently fit the TEM and MT data with the same model and resolve the shift multiplier, irrespective of its origin (in-homogeneities, topography or both).

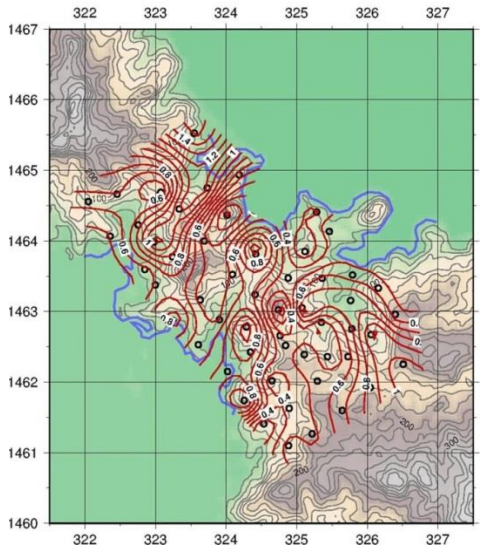


**Figure 8:** *Spatial distribution of shift multipliers and Elevation in Montelago (black circles are MT/TEM stations). Coordinates are UTM km. (Modified from Hersir et al., 2014.)*

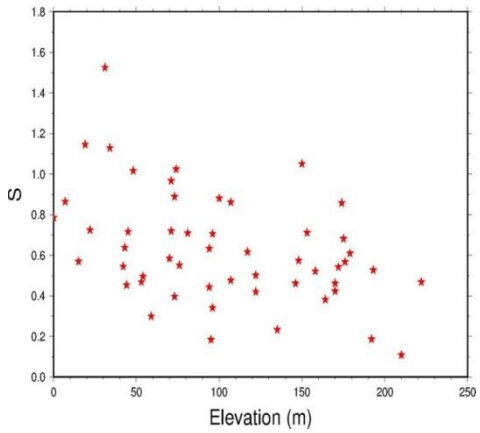


**Figure 9:** *Static shift multipliers (S) in Montelago versus elevation.*

## 2.5 Attempts to mend for static shifts

Several ways of dealing with static shifts have been proposed in the literature. An exhaustive literature survey will not be given here, but some of them are summarised by Sternberg et al. (1988). Some of these attempts make use of spatial filtering using closely spaced soundings or even continuous electric field profiling referred to as EMAP (Bostic, 1986). Jones et al. (1992) tried the assumption that at long periods the TE mode apparent resistivity should have a smooth spatial variation. Additional observations, like known thicknesses of geological units of different resistivity (from well-logs) have also been used. deGroot-Hedlin (1991) proposed to consider the shift multipliers as unknown parameters that are inverted for in 2D inversion by demanding smooth models and that the product of the shift multipliers for many soundings covering relatively large area should be close to one (sum of all shifts on log-scale zero). Ogawa and Uchida (1996) developed this idea further, by assuming that the shifts (log of shift multipliers) have Gaussian distribution around zero. Below these assumptions will be confronted with field data.

Groom and Bailey (1998) make a very interesting effort to amend distortions of the impedance tensor by local in-homogeneities close to the sounding site, by what is now generally termed as Groom-Bailey decomposition. Their approach does, however, not address the shift problem. They only deal with mixing of the components of the electric field components ("twist" and "shear") due to distortion by local resistivity anomalies but the frequency independent shift multipliers are not determined. Another weakness of their approach is that, apart from 3D local anomalies, they assume that the underplaying resistivity structures is either 1D or 2D. If this is the case, it might be worth while performing Groom-Bailey decomposition before static shift correction is done.

It is sometimes claimed that static shifts can be dealt with by resolving the very shallow resistivity structure around the dipole by measuring to high enough frequencies so that currents induced by the electromagnetic wave only penetrate shallow depths. This would hold true if the earth could be considered as a pure Ohmic conductor. But at very high frequencies other processes set in. At high frequencies the earth (rocks) does not behave like a pure Ohmic conductor. In addition to the Ohmic conduction capacitance and induced polarization effects become important.

To qualitatively understand the capacitance effect, we consider a simple electrical circuit analogy of alternating current running through parallel connected resistor of resistance, R and a capacitor of capacity, C (Figure 10). If the total current through the resistor and the capacitor is $I = I_0 \cdot e^{i\omega t}$, then the voltage is given as:

$$V = \frac{RC}{i\omega R + C} Io \cdot e^{i\omega t} \qquad (1)$$

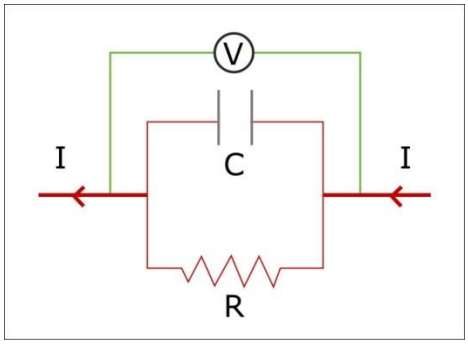


**Figure 10:** *Simple circuit analogy of capacitance effect.*

For low frequencies and low resistance R the effective resistance (impedance) is close to R and the voltage is in phase with the current. But for high frequencies and high resistance the effective resistance decreases and the voltage gets out of phase with the current. In terms of MT soundings, this means that in the case of very resistive surface layers, like dry lavas, the electric field is decreased at high frequencies making the apparent resistivity biased down and the phase gets distorted.

As mentioned earlier, the rocks in geothermal systems are subject to geothermal alteration. At temperatures lower than about 240°C the dominant alteration minerals are clay minerals and zeolites (Árnason, et al., 2000). These minerals are very conductive and form the so called low resistivity (clay) cap on the outer margins of the geothermal systems. In addition to high conductivity, clay minerals have high induced polarization (IP) capacity. The IP effect can be described as if the rocks have, in addition to galvanic conductivity, a frequency dependent complex conductivity (Bertin and Loeb, 1979):

$$\sigma = \sigma_0(1 + i\varepsilon_{IP}\omega/\sigma_0) \tag{2}$$

where $\sigma_0$ is the DC conductivity and $\varepsilon_{IP}$ is a parameter similar to a dielectric permittivity. If the current density is $j = j_0 \cdot e^{i\omega t}$ then Ohm's law gives:

$$E = \frac{\rho}{i\omega\varepsilon_{IP}\rho+1}\, jo \cdot e^{i\omega t} \tag{3}$$

where $\rho$ is the DC resistivity ($1/\sigma_0$). If $\varepsilon_{IP}$ is large (values as high as 0.8 ms/**Ω** have been reported (Bertin and Loeb, 1979)) and if the frequency is high the electric field is reduced and, like for the capacitance effect, the apparent resistivity is biased down and the phase is distorted.

The microscopic physics behind the capacitance and IP effects is similar (polarization) and equations (1) and (3) have basically the same form ($\varepsilon_{IP}$ is like inverse capacitance). These two effects are discussed separately here because the former appears due to very high surface resistivity and the latter due to high IP capacity of conductive clays.

In geothermal areas in volcanic environments very resistive surface lavas are quite common and clay alteration is also common at, or close to, the surface. It is also commonly observed, when performing joint inversion of TEM and MT data, that the MT apparent resistivity is biased down and the phase distorted at the shortest periods (highest frequencies) and the two datasets cannot be fitted with the same model. But if a few of the shortest periods of the MT are discarded, they can be nicely fitted with the same model.

## 2.6 TEM, the remedy

In the central-loop Transient Electro-Magnetic (TEM) method a loop of wire is laid on the ground and constant current transmitted in the loop. The current builds up a magnetic field of known strength. The current is then abruptly turned off. The magnetic field is left without its source and responds by inducing an image of the source loop in the surface. Due to Ohmic loss (heat), the current and the magnetic field decay and again induce currents at greater depth. The process can be visualized as if the induced currents diffuse downwards and outwards with time like a "smoke fringe" (Nabighian, 1979) as schematically shown on Figure 11. The decay rate of the magnetic field with time is measured by the induced voltage in a coil at the surface. The decay rate of the magnetic field with time is dependent on the current distribution which in turn depends on the resistivity distribution. The induced voltage in the receiver coil, as a function of time, can therefore be interpreted in terms of the subsurface resistivity structure.

It is clear from the discussion above, and has been thoroughly confirmed by model calculations (e.g. Sternberg et al, 1988), that near surface resistivity anomalies only affect the TEM at very early times. At late times the current distribution has diffused deep below near surface anomalies and their effects disappear. Similarly, topography can affect TEM at early times, but at late times, when the induced currents have diffused down below the topographic regime, the influence of the topography fates out.

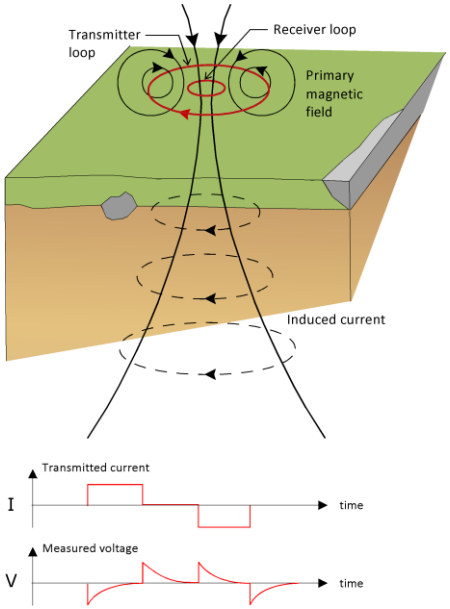


**Figure 11:** *Schematic description of a TEM sounding.*

This is fundamentally different from the MT. In the case of MT, the electric field signatures of currents induced at great depths have to be conveyed all the way to the surface and hence are prone to near surface in-homogeneities as demonstrated above and frequently, high frequency effects discussed above prohibit resolving the resistivity structure in the immediate vicinity of the electric dipoles. These properties of the MT and TEM methods have been known for a long time. In the late eighties people started to use TEM soundings to correct for static shifts in MT data (e.g. Sternberg et al., 1988). But some people still apply the MT method without proper static shift correction. This

may be justified in areas with gentle topography and where the near surface rocks are homogeneous, such as sedimentary layers. High temperature geothermal systems in volcanic areas are the other extreme. They are normally characterised by very high resistivity contrast at the surface and at shallow depths which are ideal conditions for extreme static shifts. Joint inversion of MT and TEM data at Iceland GeoSurvey has revealed shift multipliers a low as 0.1 (see below). If the shift was not corrected for, interpretation would give ten times too low resistivity values and about three times too shallow depths to resistivity contrasts. Likewise, if the MT apparent resistivity is shifted up, the interpretation will give too high resistivity values and too great depths to resistivity boundaries.

A software, named TEMTD, has been developed for joint 1D (layered earth) inversion of MT and TEM data. The software is described in deliverable D5.3. The software inverts the two datasets for both the resistivity model and the shift of the MT. The development of this software started in the IGET and 3DIM projects mentioned above and was developed further under the IMAGE project to make it a versatile and powerful tool for inversion of TEM and MT data. Besides determining the static shift, joint inversion is an important quality check of the TEM and MT data sets, i.e. weather they are compatible.

In the data collection, care has to be taken to make both TEM and MT soundings in the same place (within less than 100 m). The assumption is made that, at shallow depth, the actual resistivity structure can be approximated by a layered model. In the joint inversion, inversion is done for the model parameters and one additional parameter, a shift multiplier S of the MT apparent resistivity. S is an a priori unknown parameter by which the MT apparent resistivity values have to be divided in order to fit the MT and TEM data with the response of a common model. The joint inversion is not just an efficient and objective way of determining the shift multiplier, it is also an important compatibility check of the data. If the TEM and MT data cannot be fitted with the same model, either TEM or MT data (or both) are likely distorted and soundings may need to be repeated. It is a good practice to do such a joint inversion concurrently with the data acquisition to identify any corrupt data before leaving the field.

Figures 12 and 13 show comparison of 1D inversion of shifted MT data alone and joint inversion with TEM (the time, t, after turn-off for the TEM data has been transformed to period T according to the transformation T = t/0.2 (Sternberg et al., 1988)). In Figure 12 the MT (determinant) apparent resistivity is shifted up. The figure shows how that results in too high resistivity values and too great depths to resistivity variations (not the logarithmic model scales) when inverting the MT alone. In Figure 13 the MT apparent resistivity is heavily shifted down resulting in too low resistivity at depth and too shallow depths to resistivity variations. The figure also shows how the TEM resolves shallow low resistivity not resolved by the MT.

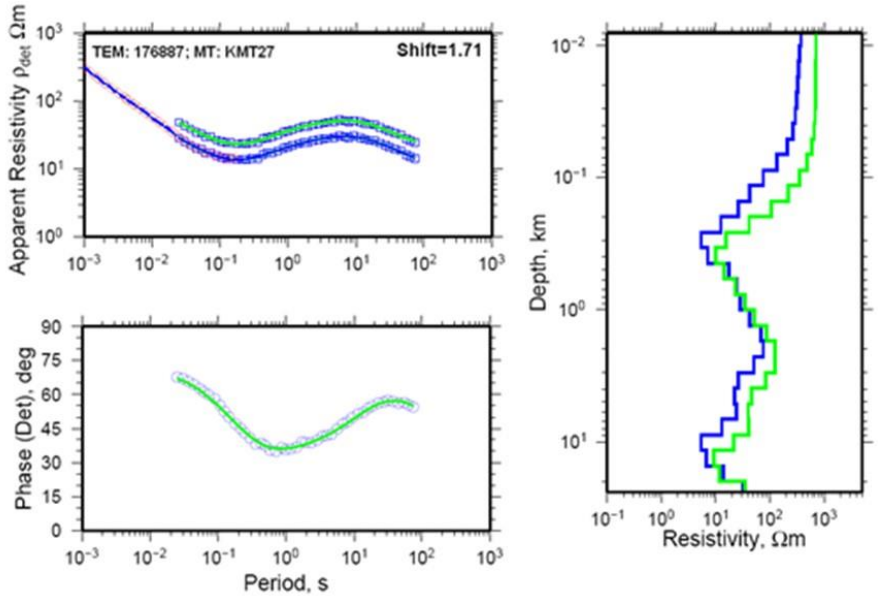


**Figure 12:** *An example of 1D inversion of MT determinant apparent resistivity and phase with apparent resistivity shifted. Inversion of the MT data alone (green solid lines in the left panels) gives the model shown in green in the right panel. Joint inversion with a nearby TEM sounding (blue lines in the apparent resistivity panel) shifts the apparent resistivity down (divided) up by a factor of 1.71 (top right corner of the apparent resistivity panel), resulting in the model shown in blue in the right hand panel (note that the depth scale is logarithmic).*

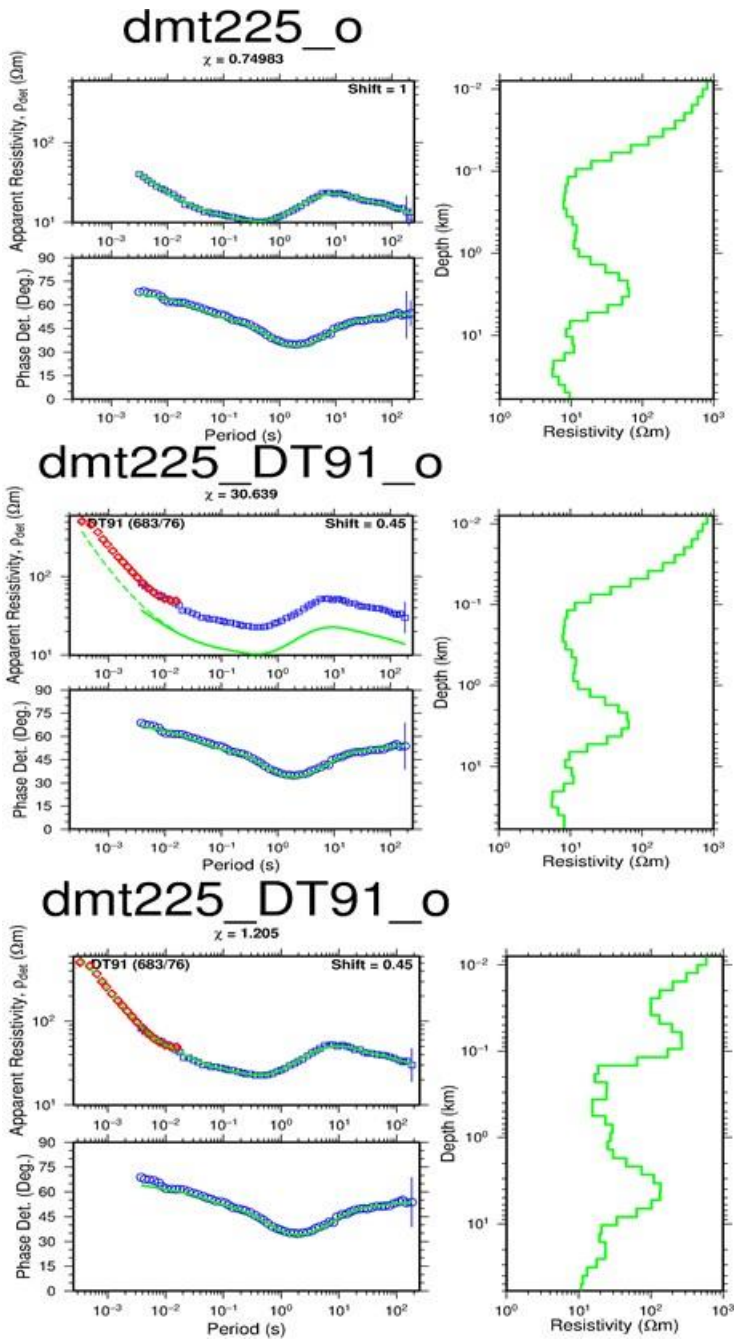


**Figure 13:** *An example of 1D inversion of MT determinant apparent resistivity and phase with apparent resistivity shifted down. MT data are shown as blue squares and TEM data as red diamonds. Green lines to the left are the calculated response of the models shown in green to the right. The top figure shows inversion of the MT alone. The middle figure shows calculated response for both TEM and MT of the model from inversion of MT alone compared to the TEM data MT and the MT data shifted up (divided) by the shift factor of 0.45 determined by joint inversion of TEM and MT shown in the bottom figure.*

Cumming and Mackie (2010) discuss the use of TEM for static shift correction of MT data. They question the applicability of TEM data collected with small loops in resistive environments. There is, however, no physical reason why TEM should not resolve the shallow resistivity structure in resistive environments, but big loops and/or large current may be needed, to make the TEM data tie in with the MT data. The TEM and MT datasets have to resolve a common depth interval.

Watts et al. (2013) and Stark et al. (2013) question the use of TEM to correct for static shifts of MT in the case of extreme topography and show how TEM can be affected by extremely narrow, steep and high ridges (or valleys). The situations they consider are rather exceptional and the example from Montelago above is considered to show that TEM can be successfully used to correct for static shifts due to very rugged topography.

## 2.7 Field examples

Below is some analysis of static shifts observed in three TEM and MT surveys in high temperature geothermal fields in volcanic complexes: The Krafla area in NE Iceland, the Hengill area in SW Iceland and the Asal Rift in Djibouti, East Africa. The first stage in the interpretation of the data is a joint 1D inversion of the TEM data and the MT determinant apparent resistivity and phase as described above. In such a joint inversion it was frequently observed that a satisfactory simultaneous fit could not be obtained for the TEM data and the shortest periods (highest frequencies) of the MT data. This is probably because the MT apparent resistivity is too low (biased down) at the high frequencies by the capacitance and/or IP effects discussed above. (The MT data are always processed using remote reference to avoid bias due to coherent noise in the magnetic field).

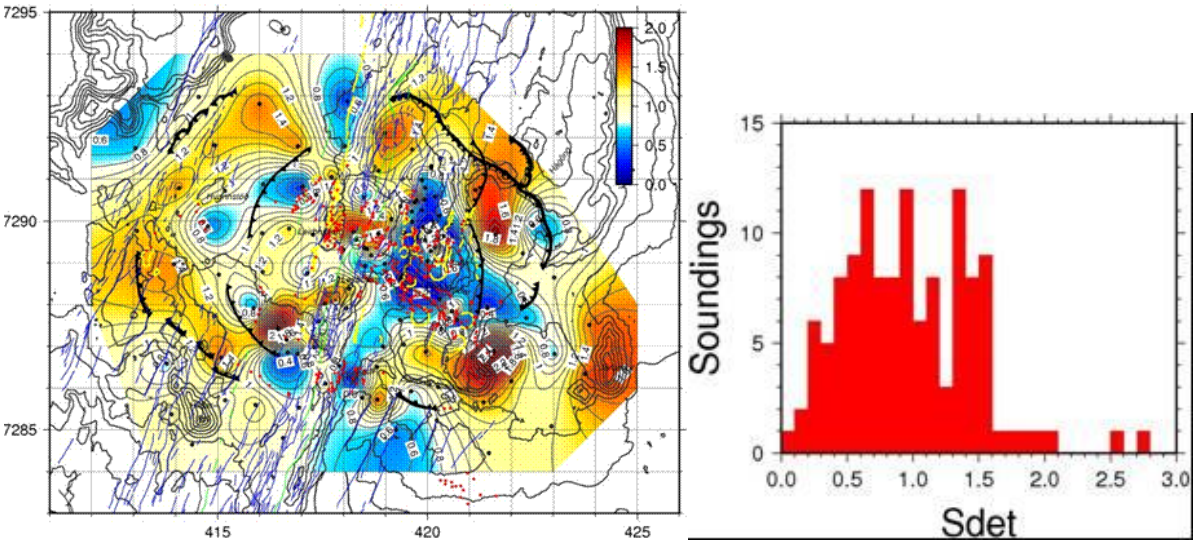


**Figure 14**: *Map showing the spatial distribution (left) and histogram (right) of shift multiplers of determinant MT apparent resistivity in the Krafla area NE Iceland (Árnason et al., 2009). Red dots on the map are geothermal surface manifestations. Coordinates are UTM km.*

Figure 14 (right) shows a histogram of the shift multipliers of the determinant apparent resistivity for 124 MT soundings in the Krafla area, north Iceland, ranging from as low as 0.1 to 2.7. It is seen that multipliers less than one (shift down) are more common than greater than one (shift up). Figure 14 (left) shows the spatial distribution of the static shift multipliers in Krafla. The Figure shows that there are shifts up in contiguous areas in the outer parts of the survey area and severe shifts down in the central part were altered rocks reach close to the surface. The survey area in Krafla is rather flat and the observed shifts cannot be due to topography.

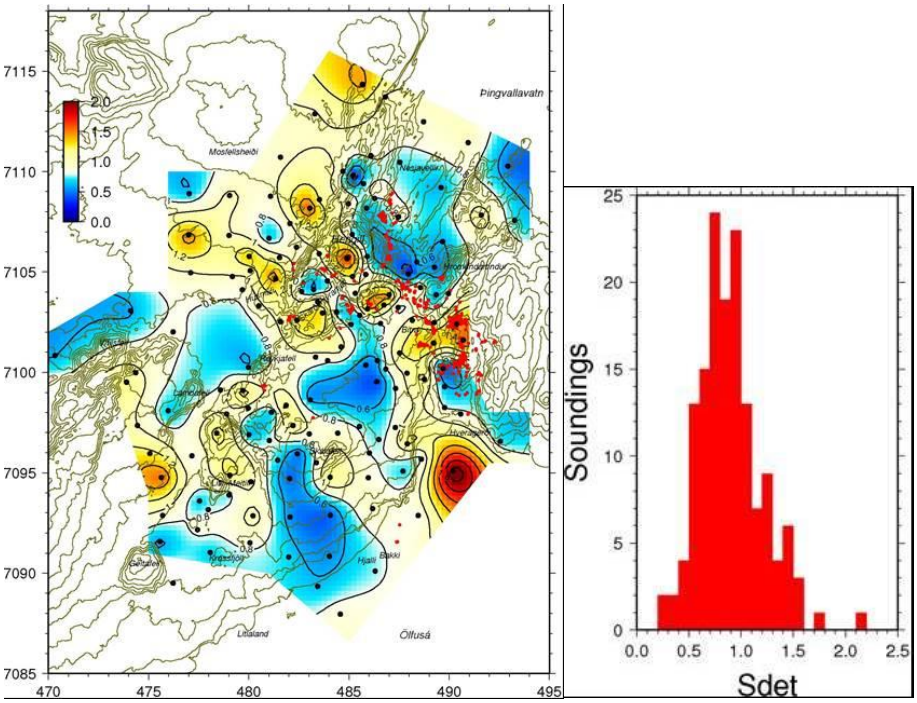


**Figure 15**: *Map showing the spatial distribution (left) and histogram (right) of shift multipliers of the determinant MT apparent resistivity in the Hengill area SW Iceland (Árnason, et al., 2010). Red dots on the map are geothermal surface manifestations. Coordinates are UTM km.*

Figure 15 shows a histogram (right) and spatial distribution (left) of the shift multipliers of the determinant apparent resistivity of 146 MT soundings in the Hengill area, SW Iceland. The shift multipliers range from 0.3 to 2.3 and again values less than one are more common than higher than one. The spatial distribution shows NW-SE trending areas with consistent shifts up or down, with the downshifts areas coinciding with surface (or near surface) alteration. The topography of the Hengill area is generally relatively gentle, except for the Hengill volcano which rises about 400 m above the surroundings. The map on Figure 15 shows no correlation between shifts and topography. On the contrary, it shows shift up along a NW-SE line crossing the mountain and shifts down to the NE and SW of the steep mountain.

The final field example is from the Asal Rift in Djibouti, East Africa. Figure 16 shows a histogram (right) and spatial distribution (left) of the shift multipliers of the determinant apparent resistivity of 64 MT soundings in the area. The shift multipliers range from 0.1 to 2.2 and once again, multipliers below one are much more common than above one. The spatial distribution shows severe shifts down in most of the survey area and few places of shifts up, mainly in the south part and the centre of the survey area. The Asal Rift is mainly a lava shield cut by, in some places big, NW-SWE trending normal faults, but relatively flat in between. There is no obvious correlation between shifts and topography seen on the map of Figure 16.

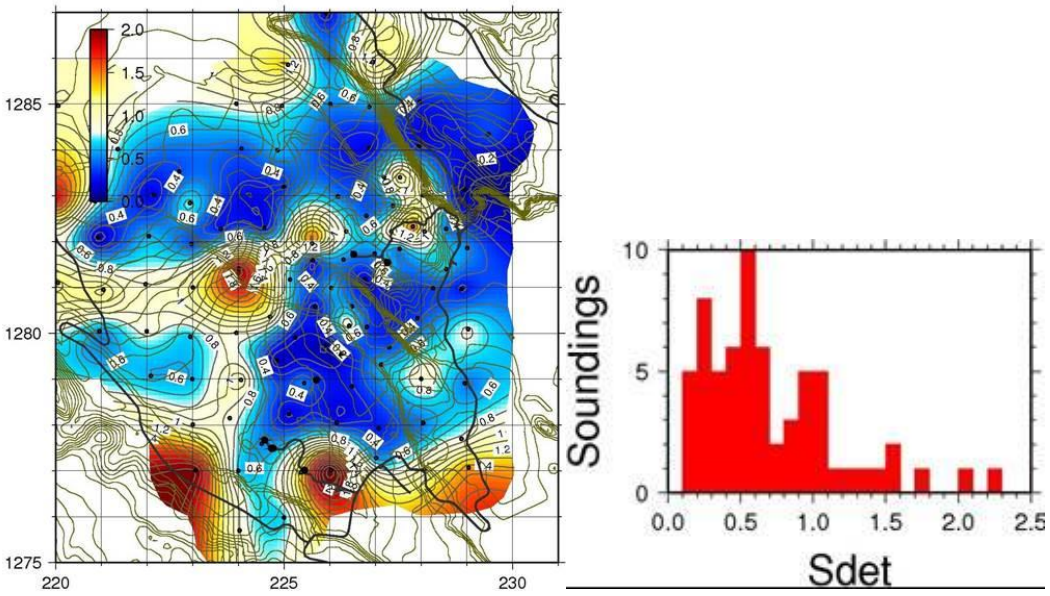


**Figure 16:** *Map showing the spatial distribution (left) and histogram (right) of shift multipliers of determinant MT apparent resistivity in the Asal Rift in Djibouti (Árnason, et al., 2010). Coordinates are UTM km.*

The maps on Figures 14, 15 and 16 show that the shift multipliers are not random, there are regions with consistent shifts, mainly shifts down. In the Krafla and Hengill areas, the MT data are consistently shifted down where geothermal alteration minerals are found on the surface or at shallow depth. In the Asal Rift in Djibouti there are large areas where the MT data are consistently shifted down. It is obvious that if the shifts are not dealt with properly, the interpretation can give very false resistivity structure.

As mentioned earlier, some of the attempts to deal with the static shifts from the MT data alone make use of spatial averaging and some statistical assumptions. deGroot-Hedlin (1991) assumes that the shift multipliers are random and that the product of the shift multipliers is close to one (the average of shifts on log-scale close to zero) for sufficiently many soundings covering large enough area. This assumption is tested in Table 1, which shows some statistics of the shift multipliers in Krafla, Hengill area and the Asal Rift.

**Table 1:** *Statistics of shift multipliers.*

| Area | Nr. of soundings | Product | Mean | Geometric mean |
|---|---|---|---|---|
| Krafla | 124 | 1.683e-10 | 0.969 | 0.834 |
| Hengill | 146 | 1.089e-10 | 0.905 | 0.855 |
| Asal Rift | 64 | 1.045e-16 | 0.702 | 0.563 |

It is evident from the Table that the assumption of deGroot-Hedlin that the product of the shift multipliers should be close to one is not valid, at least not for MT surveys in geothermal fields in volcanic areas. Different assumptions have been proposed for the statistical properties of the shifts (e.g. Ogawa and Uchida, 1996) and 2D, and even 3D, inversion including inversion for static shifts

(Sasaki and Meju, 2006). It is, however, evident in all the examples shown here, that profiles could be run in areas where all the data are severely shifted nearly in the same way and comparison to other profiles that are shifted differently has little meaning.
Table 1 shows that shifts down are more common than up. One of the reasons is probably that it is generally preferred to locate the soundings on vegetated patches with conductive soil so that the electrodes get good contact to the ground. By doing this, the data are systematically shifted down.

## 2.8 Static shift correction for 3D inversion of MT

3D inversion of MT soundings is normally done for the impedance tensor. Prior to the inversion, a static shift correction of the tensor can be done. After rotating the tensor so that the two orthogonal polarizations are along the horizontal axes of the model grid (orthogonal grids are assumed here), joint 1D inversion of the xy and yx polarizations with the nearby TEM sounding is performed to determine the shift of each polarization, Sxy and Syx. Fig 17 shows a histogram of the shift multipliers for MT soundings from the Hengill area, SW Iceland. Figure 17a shows both Sxy and Syx and Figure 17b their ratio, Sxy/Syx. Fig. 17a shows that the distribution of Sxy and Syx is broader than the distribution of multipliers of the determinant apparent resistivity (Figure 15, right). This is in accordance with what the model calculations above showed (Figures 4, 5 and 6). Fig 17b shows that the ratio Sxy/Syx ranges from 0.2 to 4, but with the majority between 0.2 and 1.8. It is interesting to see that ratios less than one are more common than higher than one. The field layout was with the x-direction in magnetic north, N16°W, but prior to the shift correction, the tensor (and derived apparent resistivity) was rotated so that the new x-direction was along the strike of the fissure swarm through the Hengill volcano, N30°A. The reason for ratios less than one being more common could be that vegetation patches are elongated along the fault direction.

If it is assumed that the shifts are mainly due to distortion of the electric fields, the corrected tensor $\mathbf{Z}^c$ can be defined as:

$$\begin{bmatrix} Z^c_{xx} & Z^c_{xy} \\ Z^c_{yx} & Z^c_{yy} \end{bmatrix} = \begin{bmatrix} C_x & 0 \\ 0 & C_y \end{bmatrix} \begin{bmatrix} Z_{xx} & Z_{xy} \\ Z_{yx} & Z_{yy} \end{bmatrix} \quad ; \quad C_x = \sqrt{1/Sxy} \; ; \; C_y = \sqrt{1/Syx}$$

This formulation is a simplification of the total static distortion discussed by Groom and Bailey (1989), where twist and shear are not considered. It is similar to the anisotropy part in the Groom-Bailey decomposition that has no control of the absolute values of Cx and Cy only of their ratio. It can be argued that this is too simplistic approach, but it must be borne in mind that there are only two independent estimated parameters at hand for the correction (estimated shift of the two polarizations) and the above procedure is the simplest using these two parameters.

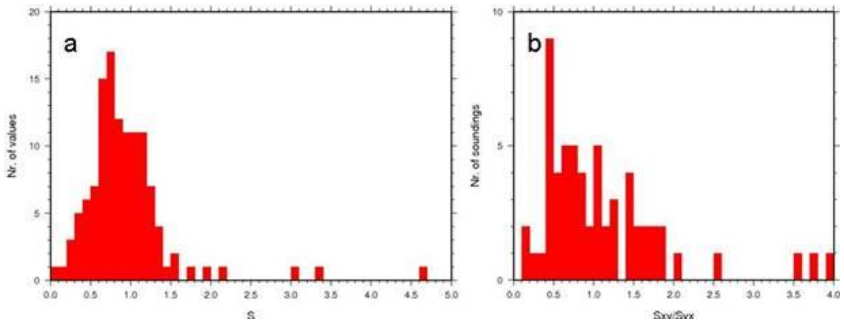


**Figure 17:** *Histogram of the shift multipliers for the xy and yx polarisations of 60 MT in the Hengill area (a) and the ratio Sxy/Syx (b).*

## 2.9 Can 3D inversion of MT correct for static shifts?

As mentioned above, some people think (and some service vendors claim) that 3D inversion of MT can correct for static shifts by inserting shallow resistivity anomalies if the topography is properly modelled. This is a bold claim not well documented in the literature and should be thoroughly tested. It was therefore decided to do so within the present work. Her such a test using MT and TEM data from the Asal Rift in Djibouti, East Africa is presented. The Asal Rift is a landward continuation of the oceanic spreading ridge of the gulf of Aden-Tadjura. The rift is characterised by a shield volcano within a graben with steep boundary faults between the gulf and Lake Asal. Lake Asal is a super saline lake at the elevation of 155 m below sea level, about 12 km NW of the bay. The central rift has gentle topography, about 200 m above sea level in the SE part of the survey area and then gently sloping towards the lake in the NW, 150 m below sea level (Figure 18).

The TEM soundings of the survey were done using 300m x 300m loops and with current about 22 A, resulting in very high data quality. Central-loop TEM soundings are extremely sensitive to the depth of a conductive layer under surficial resistive layer and 1D inversion of the TEM data resolved very well the depth to the saline groundwater. It showed that that in SE part of the central rift, the saline groundwater was at sea level, at about 200 m depth, but a little inland it drops to about the level of Lake Asal, 155 m below sea level. This drop of the water level within the active fissure swarm is explained by massive deposition of anhydrite around the geothermal system in the SE part. The thickness of the resistive surface layer, according to the TEM data, is therefore about 200 m in the SE part of the survey area, but soon increases quite sharply towards NW, to about 350 m, and further to the NW it gets gradually thinner towards Lake Asal.

A 3D inversion was done of the MT data from the Asal Rift, both of shift corrected data, as described above, and of uncorrected data. The inversion code used was WSINV3DMT (Siripunvaraporn et. al, 2005). The code assumes flat (horizontal) surface, which is justified here because of the gentle topography in the inner rift. The model grid has 400 m grid spacing (in bot horizontal directions) in the central part with data coverage and padded in all horizontal directions with ten grid planes with exponentially increasing grid spacing to a large distance. To allow the inversion the freedom to insert shallow resistivity anomalies, the vertical grid spacing was kept small near the surface (the topmost nine of them are 2, 4, 8, 16, 26, 36, 56, 50, 76 and 100 m thick) and then gradually increasing to great depths. Relatively little smoothing (regularization) was imposed in the inversion, also to allow for local shallow resistivity anomalies. The inversion was run in exactly the same way for the

uncorrected and corrected data, with an initial model of homogeneous half-space of 10 Ωm, except for the sea and Lake Asal. Bathymetry used to fix the sea at 0.2 Ωm and Lake Asal 0.1 Ωm in the models. The final fit to the data was very similar, weighted RMS of 1.6 for the uncorrected data and 1.5 for the corrected data.

Figures 19, 20 and 21 show comparison of vertical resistivity cross-sections through the resulting resistivity models. The locations of the sections are shown on Figure 18. The upper coloured sections are through the model from uncorrected data and the lower through the model from corrected data. The top panel shows estimated shift multipliers of the determinant apparent resistivity of the soundings near the profile.

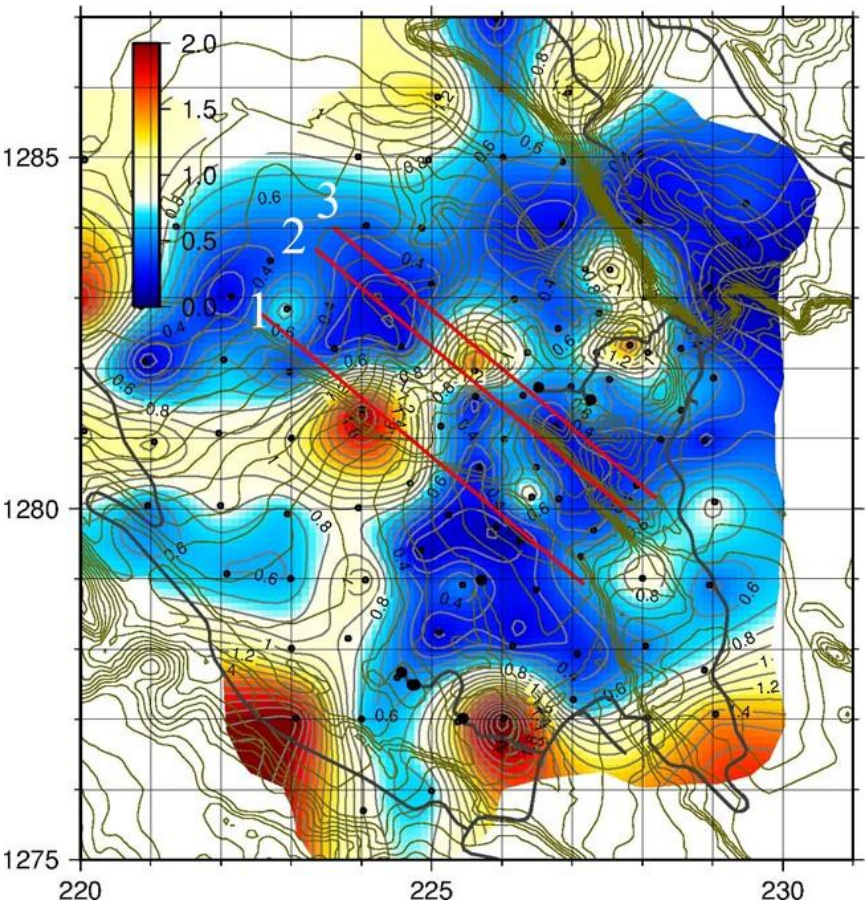


**Figure 18:** *Spatial distribution of shift multipliers of determinant MT apparent resistivity in the Asal Rift in Djibouti and location of cross-sections on figures 19, 20 and 21, through models resulting from 3D inversion of MT data without and with static shift correction***.**

Figures 19, 20 and 21 show very different models. The model from the inversion of the corrected data shows consistent and continuous high-resistivity layer in the lavas above the saline groundwater. This layer thickens from SE and then gets thinner towards Lake Asal in the NW. The thickness of the layer is comparable to that determined from the TEM data, and described above. The model from the uncorrected data, on the other hand, shows the surficial resistive layer, known to be present, extremely thin or missing in some areas. These areas correlate strongly with shift multipliers of the determinant apparent resistivity being less than one. At deeper levels, the two

models are very different. For profile 1 (Figure 19), the two models roughly agree on higher resistivity below 1 km depth between X between -2000 and 1000 m, but at shallower depth the uncorrected model is heavily distorted. For the other two sections, 2 and 3 (Figures 20 and 21) the deeper structures are completely different, one showing low resistivity where the other shows high resistivity.

This example shows that the claim that 3D inversion can deal with static shift distortion cannot be trusted. Modelling of topography can probably, to some extend account for shifts due to topography. This will, in many cases require very fine grids, which will make the computational task and memory requirements very big. The example here shows that it cannot at all be trusted that the inversion will arrange shallow resistivity anomalies to mend for shifts of that origin.

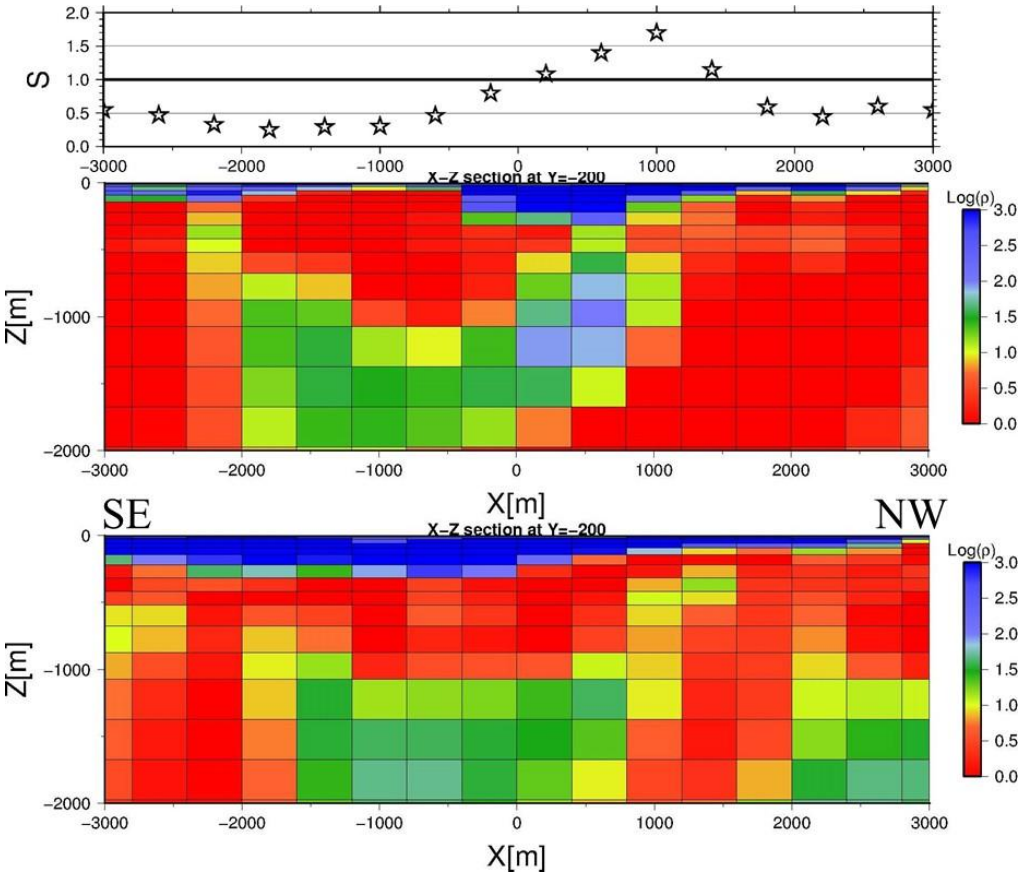


**Figure 19:** *Comparison of resistivity cross-section 1 through models resulting from 3D inversion of MT data from the Asal Rift in Djibouti, without (upper colour panel) and with static shift correction (lower colour panel). The location of the section is shown on Figure 18. The top panel shows the shift multiplier of the determinant apparent resistivity of soundings nearest to the profile.*

The problem is that 3D inversion is a severely under determined problem and some regularization is needed to give meaningful results. The standard way of doing that is to impose some sort of model smoothness. But to allow the near surface anomalies that cause the shifts, the models need to be allowed to be rough at shallow depths. This will call for some elaborate regularization schemes allowing the models to be rough near the surface (not resolved by the MT data) but smooth at depth. But the depth at which this change in smoothing should take place depends on the unresolved and

unknown shallow resistivity structure. Ad-hoc adjustment of this depth will add further ambiguities in the inversion.

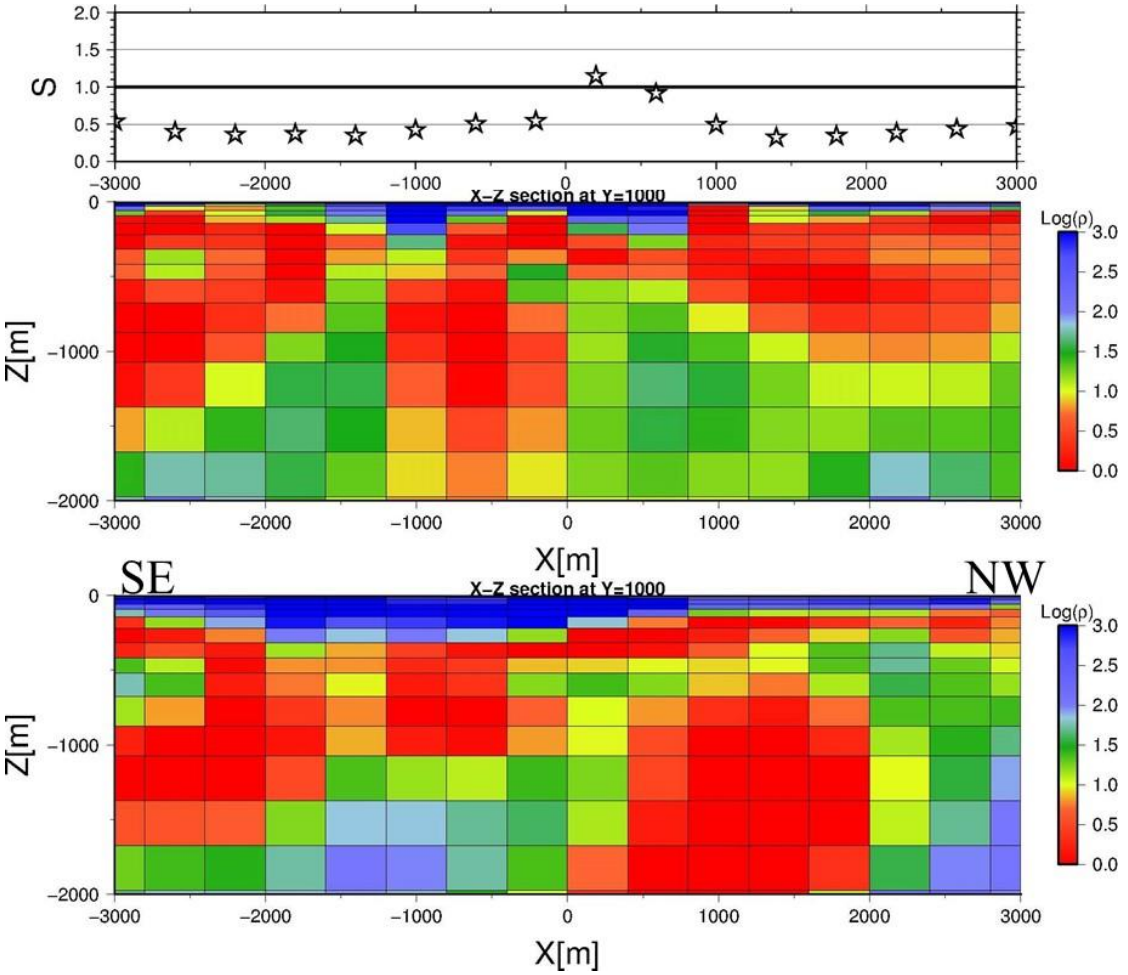


**Figure 20:** *Comparison of resistivity cross-section 2 through models resulting from 3D inversion of MT data from the Asal Rift in Djibouti, without (upper colour panel) and with static shift correction (lower colour panel). The location of the section is shown on Figure 18. The top panel shows the shift multiplier of the determinant apparent resistivity of soundings nearest to the profile.*

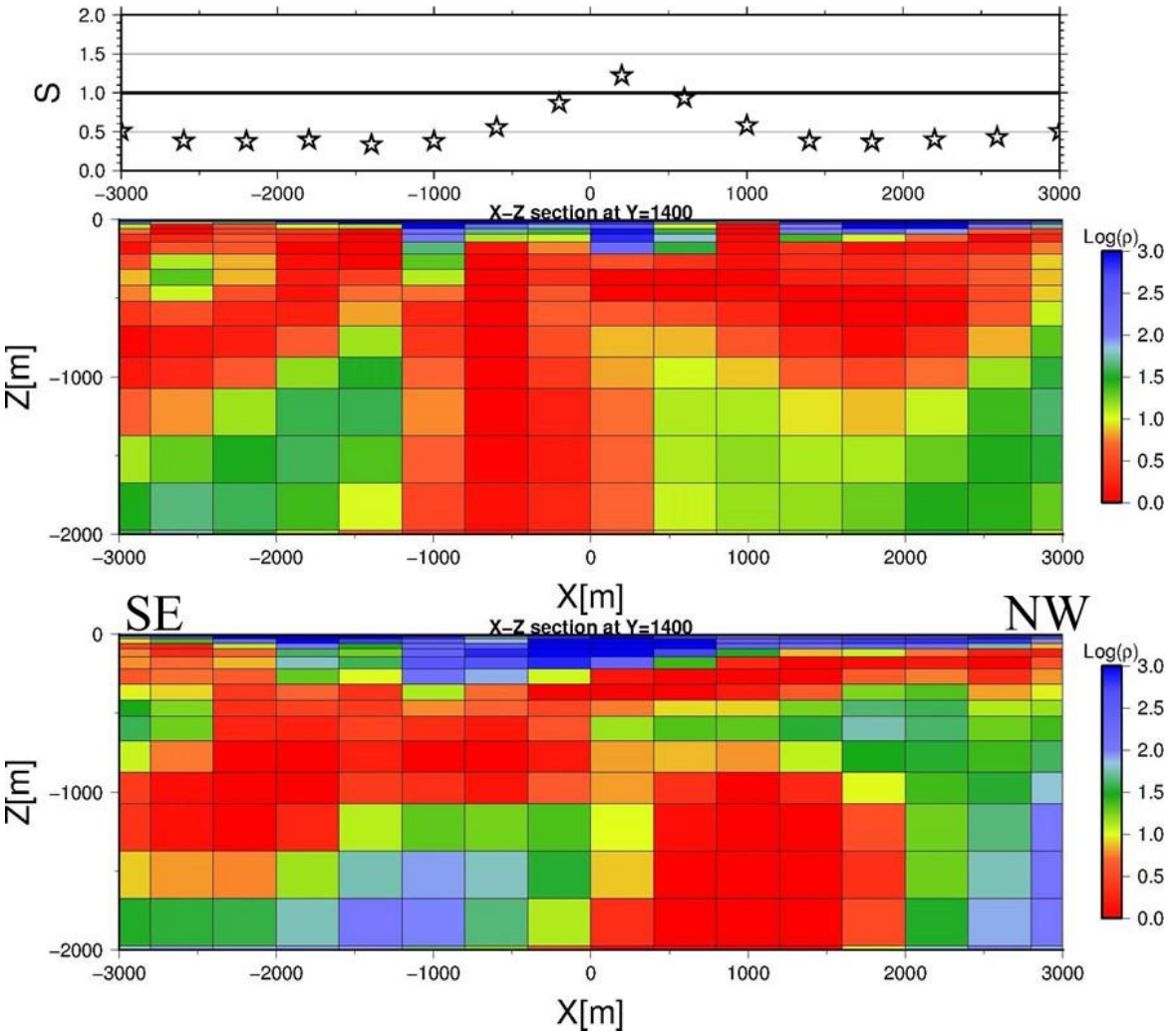


**Figure 21:** *Comparison of resistivity cross-section 3 through models resulting from 3D inversion of MT data from the Asal Rift in Djibouti, without (upper colour panel) and with static shift correction (lower colour panel). The location of the section is shown on Figure 18. The top panel shows the shift multiplier of the determinant apparent resistivity of soundings nearest to the profile.*

## 2.10 3D inversion of MT data, workflow and pitfalls

Software is now available for inversion of MT data for all the three dimensionalities, 1D, 2D and 3D, of models. 1D and 2D inversion has been used for a long time and 3D inversion has become available during the last decade. It is a common believe that 1D inversion is very robust, but giving a blurred picture. In 1D inversion individual soundings are modelled by a horizontally layered models and a pseudo 3D model is compiled by interpolation of the individual layered models. It is inevitable that assuming layered earth under each sounding will result in smeared-out models.

2D inversion has been widely used for a long time. The experience is that it can be very misleading, except in the cases where the resistivity structure is nearly two-dimensional (with well defined electric strike) and care is taken to rotate the data into TE and TM modes of that strike. If 2D profile is run to the side of a buried (low) 3D resistivity anomaly, the soundings will be influenced and 2D

inversion will inevitably place an anomaly under the profile. Therefore, if the data do not show clear and consistent electric strike, 2D inversion should not be trusted.

3D inversion of MT, if properly done, is found to sharpen the resistivity structure as compared to 1D inversion. Figure 22 shows comparison of horizontal slices through a 3D resistivity model compiled from joint 1D inversion of MT and TEM (left) and 3D inversion of static shift corrected MT in the Hengill area, SW Iceland. The 3D inversion was done using an initial model of homogeneous half-space of 50 Ωm. The Figure shows that the 3D inversion gives very similar but considerably sharper and more detailed resistivity structure than the 1D inversion.

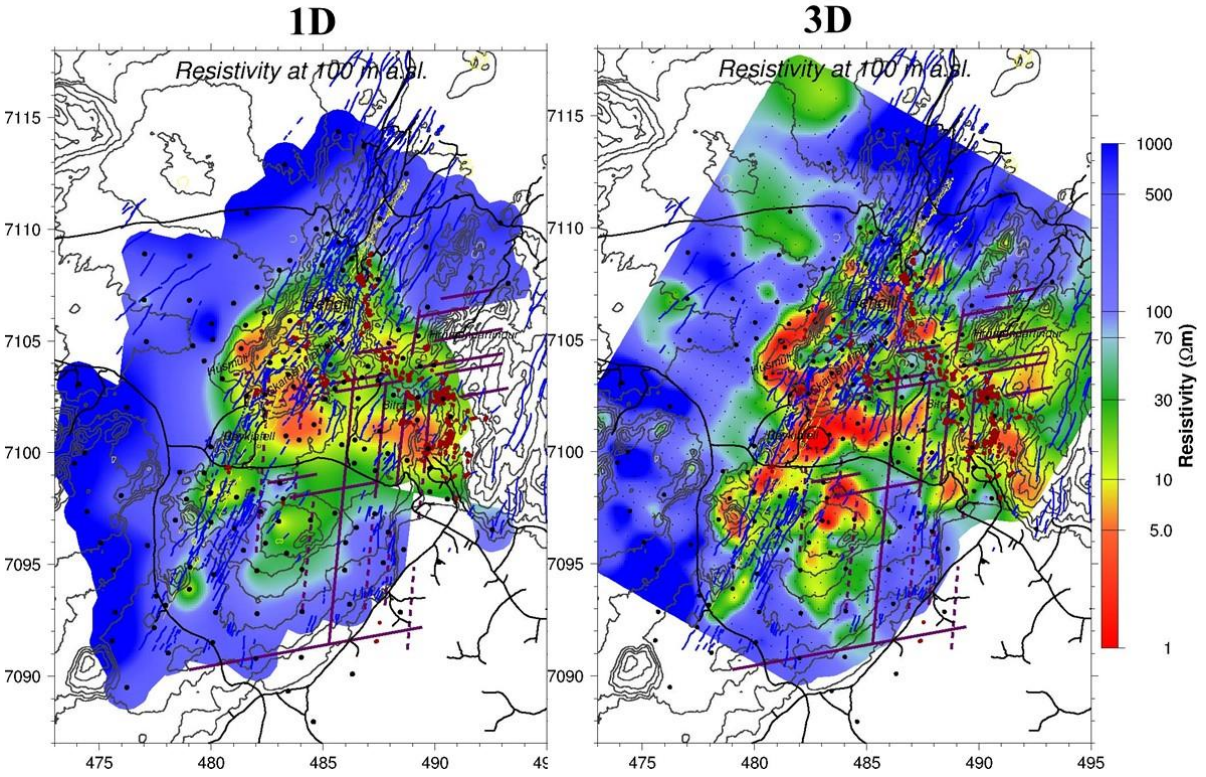


**Figure 22:** *Comparison of resistivity models from joint 1D inversion of TEM and MT (left) and 3D inversion of static shift corrected MT (right) from the Hengill are, SW Iceland Black dots show sounding locations.*

3D inversion of MT data is not a straight forward and well established process. The inversion is a huge computational task, requiring both powerful CPUs and huge memory storage. Limitations of computational facilities lead to trade-offs, such as the number of soundings to invert, number of data values for each sounding i.e. number of frequencies and parameters to invert for (off-diagonal tensor elements, full tensor, tensor and tipper) and grid size (number of grid cells). A sort of "best" practice is thought to contain following steps:

1. **Select the soundings to be inverted**. This may be necessary if the number of available MT soundings in the area to be studied is high, making inversion of all of them too big a computational task. Further, if the station density is very un-even, with dense soundings in part(s) of the area to be modelled but coarser in other parts, some of the stations in the dense

part should be omitted. The ideal situation is to have equidistant regular station coverage of the area to be resolved by the inversion.

2. **Rotate the MT data to geological or electrical strike, if known.** Most codes used in 3D inversion of MT data use finite difference code for forward calculations, using rectangular grids. If favoured directions of resistivity boundaries are expected, aligning grid axes along these directions will help in making the models more regular, avoiding zigzag boundaries.

3. **Joint 1D inversion of xy- and yx-polarizations of each MT sounding with co-located TEM sounding to determine the shift multipliers**.

4. **Choose periods and parameters (tensor element, tipper) to be inverted**. The choice of periods is a trade off between computational cost on the one hand and resolution and depth of investigation on the other. Generally the MT data are densely sampled in periods. For physical consistency, the MT tensor must be a smooth function of the logarithm of the period (Weidelt, 1972). Inverting for five to six periods per decade is generally considered to give enough resolution. The period range and the resistivity determine the depth range of exploration. The shorter the period and lower the resistivity, the shallower resistivity structures can be resolved and the longer the period and the higher the resistivity, the deeper structures can be resolved. Typical period range is from 0.01s to 1000s.

5. **Resample the tensor (and tipper) at the chosen periods**. As the MT data are normally sampled much denser than is used in the inversion (see above) the data have to be resampled, both the tensor elements and their variances. The tensor elements can be resampled by cubic spline, but the variances can vary irregularly, especially in and around the "dead band" and linear interpolation can be a better option. Some inversion codes require that all the soundings have data values for all the inverted periods. Sometimes the measured data don't have values for the whole period range or have gaps. In this case, the data have to be linearly interpolated or padded. But care must be taken that these face data should not contribute to the weighted RMS misfit (see below).

6. **Static shift correct the tensor.** This is very critical as demonstrated above. The recommended procedure for the correction is described above. The tipper does not need to be corrected because distortion of the magnetic field by Eddy currents at shallow depths are negligible at the shortest periods of the range used in normal MT.

7. **Set up the model grid**. This is a critical step. The design of the grid is a trade-off between computational accuracy and resolution on one hand and computational cost and memory need on the other. As most of the 3D inversion codes use finite difference methods to calculate the response for a given model, the model grid is generally rectangular grid. Normally, the horizontal grid lines (vertical boundaries) make regular and "dense" square grid with equal grid spacing in both horizontal directions in the area of data coverage. The grid spacing in the dense part of the grid depends on the density of soundings and the

desired resolution. Outside the dense grid, the lateral grid spacing is normally taken to increase exponentially, e.g. by a factor of 1.2 to 1.4 in each step, out to long distances, to avoid influence form the model boundaries. Likewise, the vertical grid spacing should be dense close to the surface, but since the resolution decreases exponentially with depth, the vertical grid spacing is normally taken to increase exponentially (by a factor of 1.2 to 1.4 ) below a few hundred meters. Different periods penetrate different depths; short periods attenuate at shallow depth while long periods penetrate deep. The attenuation depth is estimated by the skin-depth (proportional to the square root of resistivity times the period). In order to maintain computational accuracy, care should be taken to ensure that there are at least three grid-planes above the skin-depth of the shortest period to be inverted. The near surface resistivity can be estimated by the joint 1D inversion of the MT data and co-located TEM sounding.

8. **Set up initial model**. As mentioned above, some people (and service vendors) believe that topography should be modelled to deal with static shifts due to topography and the inversion could take care of shifts due to near surface anomalies. It is, however, demonstrated above that this cannot be trusted and, at least in some cases, wrong, leading to erroneous models. The fact is that static shifts are caused both by topography and surficial anomalies and the two effects cannot be separated. The correlation between shifts and topography on Figure 9, demonstrates that the joint inversion does, at least partially, correct for the shifts of the two different origins. The example from the Asal Rift above shows that correction by TEM is really needed to get trustworthy models. The correction will also correct for shifts due to topography. Correcting for static shifts by TEM and modelling topography in the inversion will account twice for the topography. Most of the available 3D inversion codes offer the possibility of fixing some parts of the model with a priory given (known) resistivity values. If an MT survey is done close to the sea, bathymetry must be used to set and fix the resistivity of model cells in the sea to that of the sea (about 0.3 Ωm). 3D inversion of MT data is an iterative process and the final model, to which the iteration converges, will depend on the initial (starting) model. It is therefore a good practice, as will be discussed below, to run inversion with different initial models.

9. **Run the inversion**

There are normally several parameters that can be adjusted in the inversion. As discussed above, the inversion needs some sort of regularization. This is done by minimizing a potential (penalty function) containing not just the misfit between measured and calculated response, but also term(s) just depending on the model. All inversion codes implement some sort of smoothness criteria. Typical such criteria are a penalty for large first and/or second order derivatives in the model space. Some codes implement smoothing differently, but all smoothing criteria are intimately linked with the structure of the model grid, i.e. the size of the grid blocks. The weight of the smoothness criteria in the penalty function can normally be adjusted in the inversion. The smoothing criteria will affect the resolution and fitting of the data. Too much smoothing will decrease the resolution and may prohibit good fit to the data. Too little smoothing can result in unrealistic models and overfitting of the data. There is no general rule of how to adjust the smoothing and the fact is, that the problem of the non-uniqueness of the models has been turned into an “art” of smoothing, mostly based on experience.

Some inversion codes offer the possibility of using a prior model. In this case, the potential is taken to penalize for having the model deviate too much from the prior model. This is desirable because it can prevent artefacts to be introduced in the parts of the model not very well resolved by the data. When using a prior model, the Inversion will eventually stop decreasing the misfit because the model is deviating too much from the prior model. The model can, however, be refined and the misfit decreased by doing a second run with the best model from the previous iteration run as initial and prior model. In this way the constraints of the prior model can be gradually relaxed.

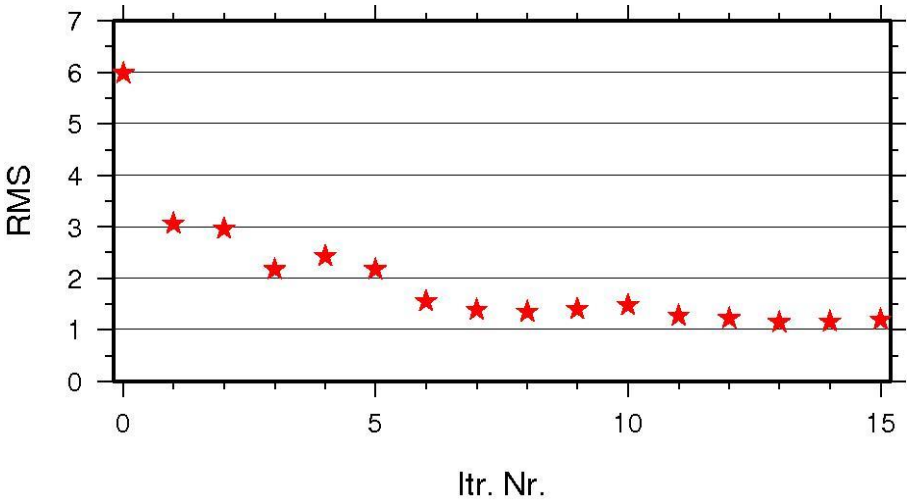


**Figure 23:** *Typical development of the RMS misfit in 3D inversion with prior models. The misfit at iteration 0 is for the response of the initial model.*

Figure 23 shows a typical development of the RMS misfit in 3D inversion with prior models. The inversion was done in three runs with five iterations in each run. In the next run the best model of the previous run was used as initial and prior model. The figure shows how the misfit n each run decreases in the beginning but then levels out in further iterations.

It may be tempting to reduce memory requirements, to try to have the model grid with as few grid planes outside the finely divided part. This should be avoided because this will decrease the accuracy of forward calculations. It is a good practice to test the grid by calculating the response of simple layered models for all sounding locations to be inverted for and compare to analytic solutions. The finely divided grid should cover all the soundings to be inverted. If soundings are located in domains of the coarser grid, insufficient accuracy in the forward solution can lead to unrealistic anomalies outside the dense grid. In the case of dense soundings in an area of interest, surrounded by more coarse station distribution, it should be considered to invert a subset of the dense soundings and the surrounding soundings on a relatively coarse grid covering all the soundings to get the regional main structures. Then resample the coarse model into a refined grid in the area of dense coverage and omit the soundings outside the dense part of the refined grid and even fix the model far outside, in a second inversion.
It has been suggested, as a good practice, to invert first for the long periods to get the big structures and then add the shorter periods to resolve shallow finer structures. This is not recommended

because experience has shown that this may cause the inversion to insert big unrealistic anomalies in the coarse part of the grid, far away from the area of interest, but still affecting the longest periods. As has been emphasised above, one of the main pitfalls is that the inversion inserts big unrealistic anomalies in the voluminous sells in the coarse padding grid. Therefore, the whole model should be plotted and inspected, not just the dense part under the area of data coverage. If such anomalies are observed, they should be rectified to reasonable resistivity values and even fixed in the model.

## 2.11 Conclusions

It has been demonstrated that static shifts of MT data collected for geothermal exploration in volcanic environment can be a big problem. The shifts can be due to shallow resistivity in-homogeneities and topography. The former reason seems to be the dominant factor with the topographic effects superimposed. The shifts often affect soundings in relatively large contiguous areas in similar way. It is therefore clear that interpretation of MT data without properly accounting for the shifts can lead to seriously wrong resistivity models. It is demonstrated that joint inversion MT with a TEM sounding at the same place is an effective and consistent way to correct for the shifts. After 3D inversion of large MT datasets became available some service vendors tend to claim that static shifts can be dealt with by the inversion. This has, however, not been convincingly demonstrated in the literature to the author's knowledge. 3D inversion of MT data is a severely underdetermined problem and regularisation of the model is needed. Some sort of smoothness criteria is generally a part of the regularisation. But to deal with near surface anomalies, like the ones encountered in volcanic areas, the models need to be allowed to have considerable roughness in the near surface. Demanding smoothness at depth while allowing roughness near the surface calls for elaborate regularisation schemes and the resulting model will likely depend strongly on the scheme chosen. It is the view of the author that joint inversion with TEM is the safest and most consistent way to correct for static shift in MT data. As discussed above, this will also correct for shifts due to topography. A consequence of this is that if the MT data are shift corrected this way, topography should not be modelled in 2D or 3D inversion. This would account twice for the topography.
The author has experienced clients tempted by saving on geothermal exploration by not doing TEM soundings along with MT. But is should be kept in mind that resistivity models from MT surveys are often the basis for decisions on big investments in drilling. Saving on the cheap surface exploration resulting in misleading models can end up as very costly.

## 2.12 References

Árnason, K.: *TEMTD a program for 1D inversion of TEM and MT data*. Short manual. ISOR internal report (2006), 17 pp.

Árnason, K., Eysteinsson, H. and Vilhjálmsson, A. M.: *The Asal geothermal field, Djibouti. Geophysical surface exploration 2007–2008.* Iceland GeoSurvey, ÍSOR-2008/019 (2008), 74 pp.

Árnason, K., Eysteinsson, H. and Hersir, G. P.: Joint 1D inversion of TEM and MT data and 3D inversion of MT data in the Hengill area SW Iceland. *Geothermics* **39**, (2010), 13-34.

Árnason, K., Karlsdóttir, R., Eysteinsson, H., Flóvenz, Ó.G., Guðlaugsson, S.Th.: The resistivity structure of high-temperature geothermal systems in Iceland. *Proceedings of the WGC 2000, Japan* (2000), 923-928.

Árnason, K., Vilhjálmsson, A.M. and Björnsdóttir, Þ.: *A study of the Krafla volcano using gravity, micro earthquake and MT data.* Iceland GeoSurvey report, ISOR-2009/067, (2009), 66 pp.

Bertin, J. and Loeb, J.: *Experimental and Theoretical of Induced Polarization, Vol. 1 and 2*, Gerüder Borntraeger, Berlin (1976).

Bostic. F. X.: *Electromagnetic Array Profiling (EMAP)*. 56th Ann. Mth. Soc. Expl. Geophys., Extended Abstracs (1986), 60-61.

Cumming, W. and Mackie, R.: Resistivity Imaging of Geothermal Resources Using 1D, 2D and 3D Inversion and TDEM Static Shift Correction Illustrated by Glass Mountain Case History. *Proceedings World Geothermal Congress, Bali, Indonesia*, April 2010, (2010), 25-29.

deGroot-Hedlin, G.: Removal of static shift in two dimensions by regularised inversion. *Geophysics*, **Vol. 56**, (1981), 2102-2106.

Jones, A. G., Gough, D. I., Kurtz, R. D., DeLaurier, J. M., Boerner, D. E., Ceraven, J. A., Ellis, R. G. and MvNeice, G. W.: Electromagnetic images of regional structure in the southern Canadian Cordillera. *Geophys. Res. Lett*., **12**, (1992), 2373-2376.

Groom, R. W. and Bailey, R. C.: Decomposition of Magnetotelluric Impedance Tensor in the Presence of Local Three-Dimensional Galvanic Distortion. *JOURNAL of GEOPHYS. RES*., **Vol. 94**, No B2 (1989), 1913-1925.

Hersir, G. P., Árnason, K. and Vilhjálmsson, A. M.: *Resistivity Survey in Montelago on Mindoro Island, Philippines. Data Acquisition, Processing and 1D inversion.* ÍSOR report, ÍSOR-2014/015, (2014), 30 pp.

Nabighian, M. N.: Quasi-static transient response of a conductive half-space. An approximate representation. *Geophysics*, **49**, (1979), 1700-1705.

Ogawa, Y. and Ushida, T.: A two-dimensional magnetotelluric inversion assuming Gaussian static shift. *Geopys. J. Int*., **126**, (1996), 69-76.

Sasaki, Y and Meju, M. A.: Three-dimensional joint inversion for magnetotelluric resistivity and static shift in complex media. *Journal of Geophys. Res*., **Vol. 111**, (2006), 1-11.

Sternberg, B. K., Washburne, J. C. and Pellerin, L.: Correction for the static shift in magnetotellurics using transient electromagnetic soundings. *Geophysics*, **Vol. 53**, (1988), 1459-1468.

Siripunvaraporn, W., Egbert, G., Lenbury Y. and Uyeshima, M.: Three-dimensional magnetotelluric inversion: data-space method. *Phys. of the Earth and Plan. Int*. **150**, (2005), 3-14.

Stark, M. A., Soyer, W., Hallinan, S. and Watts, M .D.: Distortion Effects on Magnetotelluric Sounding Data Investigated by 3D Modelling of High-Resolution Topography. *GRC Annual Meeting Extended Abstracts* (2013), 12 pp.

Watts, M. D., Mackie, R., Scholl, C. and Hallinan, S.: Limitations of MT static shift correction using time-domain EM data. *SEG Houston 2013 Annual Meeting* (2013), 681-684.

# 3 Part Two: External constraints with geophysical datasets

## 3.1 Introduction

External constraints with geophysical datasets include information on resistivity from boreholes (Section 3.2.1) and location of the brittle-ductile boundary from seismic data (Section 3.2.2). Here, the depth-location of the low-resistivity anomaly, as observed from borehole data, is build into the starting model, giving the program a headstart into gaining information on the resistivity in the survey area. Information on the ductile-brittle bounday location is used to infer the location of a deep low-resistivity anomaly, which is put into the starting model of the inversion.

## 3.2 Constraints from other geophysical datasets

### 3.2.1 Resistivity from boreholes

Borehole data provide important information about rock properties in the subsurface. Unlike the knowledge of the Earth gathered from surface exploration, where information is obtained through various modeling techniques, borehole data provide direct measurements of the numerous properties of the subsurface.

One set of measurements often included in borhole logging is resistivity. These informations are very valuable to the resistivity modeling based on surface measurements, as models can be compared to the measurements. Moreover, these information can be used as a-priori information for the resistivity models. It is, however, not obvious how one can implement information such as these into the model. In order to explore different option we create a synthetic model immitating the resistivity structure of a high-temperature geothermal system (see Figure 1). Three locations along the profile are selected to represent synthetic boreholes. At these locations the exact depth range of the low-resistivity cap is known, as is at borehole locations.

Two a-priori strategies are implemented 1) fixing the depth range of the low-resistivity cap at the locations of the synthetic boreholes by putting these into the starting model as would be done with information from boreholes; this model is referred to as the DISCRETE model (Figure 2); 2) creating a continuous low-resistivity cap by interpolating between the three synthetic borehole locations; this model is referred to as the CONTINUOUS model (Figure 3). Below we discuss the results of the two synthetic examples.

### 3.2.2 Description of the synthetic model and the model grid

Figure 1 shows a cross-section of the synthetic model which represents the resistivity structure of high-temperature geothermal systems. At the top there is a high resistive layer (500 Ωm), then the low-resistivity cap (5 Ωm ) followed by a resistive layer (200 Ωm). This sequence of resistivity

structure is attributed to the alteration of clay minerals (see e.g. Árnason et al., 2000). Further below is a deep low-resistivity layer (5 Ωm), as observed under most of Iceland (excluding the Reykjanes Peninsula), bulging up underneath the center of the area. The deepest layer is of a medium resistivity (50 Ωm).

The model is 2 dimensional and is symmetric around y=0. The structure is the same along the x-axis, such that all cross-sections perpendicular to the x-axis always gives the same structure. Although the structure of the model is 2D its response and the inversion is calculated using a 3D code and the grid designed is, therefore, also 3D.

The grid, on which the high-termperature geothermal model was designed on, had 48 cells in x and y-directions and 56 layers in the vertical direction. The main high-temperature geothermal structure spanned 8 km along the y-axis, and the the grid-spacing was 500 meters in this area. The grid-spacing then grew exponentially outside the finely-gridded area. Outside the finely-gridded area the structure was kept layered, as seen outside 4000 m and -4000 m of the model in Figure 1.
The grid spacings in the x-direction was the same as that in the y-direction but, as mentnioned above, the geothermal resistivity structure was the same along the x-axis. The grid spacing in the z-direction were as follows (in meters):

30 30 30 30 30 30 30 30 40 40 50 50 50 50 50 50 100 100 100 100 100 100 100 100 100 100 100 125 125 150 190 190 250 250 250 250 250 250 250 250 250 450 675

After this the thicknesses grew exponentailly with the thickest layer of 15716 meters.

### 3.2.3 Inversion scheme

The 3D inversion was performed using the inversion program WSINV3DMT written by Prof. Weerachai Siripunvaraporn (Siripunvarporn et al., 2005; Siripunvaraporn and Egbert, 2009). WSINV3DMT uses finite difference forward algorithm and utilizes a formulation of the inverse problem in the data-space rather than in the model-space. This reduces the dimensionality of the problem dramatically and makes 3D inversion of MT data attainable.

Starting and prior models are implemented in the methodology. The starting model defines the structure at the start of the first iteration of the inversion. In the calculations, the misfit between measured data and calculated response from the model, and the deviation of the model from the prior model, are minimized. Because of the latter regularization, the inversion seeks to maintain any resistivity structure present in the prior model and we therefore try different starting/prior models. In this work the prior- and starting models are the same within an inversion run (consisting of a few iterations) but they differ between runs. After a few iterations (usually 3-5) the resulting best model is used as the initial and prior model for the next run and the best model from that run is used as the initial and prior model for the next run, and so forth.

The synthetic MT-stations are spaced every 500 m along the y-axis and every 1500 meters along the x-axis in the 8 km x 8 km area where the grid spacing is 500 meters. The total number of synthetic stations is therefore 16x6=96.

### 3.2.4 Results of the DISCRETE model

Figure 2 shows the starting (and prior) model used for the DISCRETE model. The three artificial boreholes are given the initial value of 5 Ωm and the background resistivity is 50 Ωm.

**Table 1:** *RMS values after each run for the DISCRETE model*

| RUN NUMBER | RMS VALUE |
|---|---|
| **0** | 14.25 |
| **1** | 3.41 |
| **2** | 1.44 |
| **3** | 0.85 |

Table 1 shows the root-mean-square value after each run. It starts out with a RMS value of 14.25 and ends with a RMS value of 0.85 after 3 runs. Each run was three iterations. Figures 4 and 5 show the inversion results of the DISCRETE model down to 10 km and 4 km, respectively, after each run.

After each run, the best model was checked and if the resistivity value in the synthetic boreholes did not stay between 3 and 7 Ωm then the resistivity value of that block was set to 5 Ωm. This was done to ensure that the priori information continued into next runs.

The depth to the deeper low-resistivity layer is well resolved but it is thickner and the resistivity value larger than in the original model. Interestingly, the up-doming structure of the deeper low-resistivity layer in the input model is not recovered in the final model (Figure 4C).

The depth down to the low-resistivity cap is well defined and, as in the case of the deeper low-resistivity layer, the low-resisitivity cap is thicker and with higher values than in the input model. The synthetic boreholes are indicative of the thickness of the low-resistivity cap at their locations. A zone of intermediate resistivity is present below the synthetic boreholes, where higher-resistivity should be present, according to the mineral alteration. A different inverson scheme might be considered; where the zone immediately above and below the synthetic boreholes is locked into higher resistivity values. Note that the two outer most synthetic boreholes still have low-resistivity values whereas the one located at y=-750 m has, for the most part, been changed to having higher values than it should have.

### 3.2.5 Results of the CONTINUOUS model

Figure 3 shows the starting (and prior) model used for the CONTINUOUS model. The three artificial boreholes are given the initial value of 5 Ωm and the background resistivity is 50 Ωm. An attempt to connect the three artificial boreholes was made, resulting in a continuous low-resistivity cap. Outside the y=±4000 m the low-resistivity cap was assumed to be flat with a constant thickness, as there were no measurements outside this range.

Table 2 shows the root-mean-square value after each run. It starts out with a RMS value of 5.25 and ends with a RMS value of 0.36 after 2 runs. Each run was three iterations. Figures 6 and 7 show the inversion results of the DISCRETE model down to 10 km and 4 km, respectively, after each run.

**Table 2**: *RMS values after each run for the CONTINUOUS model*

| RUN NUMBER | RMS VALUE |
|---|---|
| **0** | 5.25 |
| **1** | 2.31 |
| **2** | 0.36 |

As in the DISCRETE model, the depth down to the low-resistivity cap is well defined. The prior model was not tinkered with between runs, as with the DISCRETE model, instead the low-resistivity cap was allowed evolve in the inversion. The rough shape of the low-resistivity cap in the input model seems to be emerging in the resulting model after 2 runs (Figure 7B).

### 3.2.6 Comparison between the DISCRETE and CONTINUOUS models

Although the low-resistiviyt cap in the starting model did not replicate the one in the input model, this model converged faster then the DISCRETE model.

By connecting the synthetic borehole locations in the CONTINUOUS model the inversion is given a head start, starting with a RMS value of 5.25, compared to 14.25 in the DISCRETE model.

In both the models, the depth to the deeper low-resistivity layer is well determined, which is thicker and of higher resistivity than the input model. Also, the up-doming of the layer is not resolved in neither of the models. Therefore, we conclude that resolving the deeper parts better using borehole data is not achieved. However, the deeper low-resistiviy layer after the 1st run in the CONTINUOUS model, so if time is an essence this might be a good inversion stradegy, provided that the data from the boreholes are of good quality and thereby reliable.

In CONTINUOUS model the constraints where such that the low-resistivity cap did not grow thicker, it stayed within the bounds of the thickness of the input model. In the DISCRETE model, however, the low-resistivity cap grew as thick as needed to fit the data. A thin low-resistivity cap with a low resistivity gives the same results as a slightly thicker cap with higher resistivity. This trade off is clearly seen in the results described here.

The results of the DISCRETE model exhibted a thicker low-resistiviy cap with a higher resistivity value compared to the input model. On the contrary, the results of the CONTINUOUS model revieled a low-resistivity cap in a fairly good agreement with the input model. Using the knowledge that the low-resistivity cap domes up, gets a little bit thinner toward the center of the geothermal system and that the it has a certain resistivity, guided the inversion very well. Assuming that these are facts, then it can be recommende to create one continuous low-resistivity cap rather than inputing only the discrete boreholes into the starting model, in roder to get a more realistic image of the low-resistivity cap.

## 3.3 Ductile-brittle boundary based on seismic data

The deep low resistivity layer, present underneath most of Iceland (excluding the Reykjanes Peninsula), domes up at the locus of rifting, underneath high-temperature geothermal systems (References?). Recently, a seismic study of the Námafjall area, north Iceland (Figure 8) revieled an aseismic zone underneath the local high-temperature geothermal system, in the form of a dome (Kristjánsson et al. (2016)) (Figure 9).

In the same area, a resistivity model (for location see Figure 10) revieled up-doming of the deep low-resistivity layer (Karlsdóttir et al. (2012)). (Figure 11). Either these two up-doming features, of the completely independent datasets, are coincidences or they are somehow related. Assuming a relation between the two, the question arises what causes the deeper low-resistivity layer to dome up. As the aseismic layer in the seismic dataset marks the boundary of the ductile-brittle boundary, it is straight forward to conclude that the up-doming of the deep low-resistivity layer has the same origin.

Assuming this connection, one can state that these two anomalies should have the same location. That is not the case as the seismic anomaly is located just to the west of the resistivity anomaly. This might be due to inaccuracies in one of the models. Nevertheless, the seismic data can be used as apriori information in the resistivity modeling, assuming that the updoming of the aseismic area deliniates the low-resistivity up-doming.

Figure 11 shows the relationship between these two datasets. The blue circle, outlines the aseismic area, which falls inline with the location of the up-doming of the deep low-resistivity anomaly. In order to use the seismic data as apriori information, a structure is implemented into the prior/starting model, as in the synthetic borehole example, to immitade the up-doming of the seismic data. Figure 12 shows the startin/prior model of the inversion. The deep low-resistivity anomaly (5 Ωm) is fixed to a depth of 7500 m to 11000 m below sea level. The up-doming is then deigned to fit the seismic data and the resistivity value surrounding the low-resistivity structure is 70 Ωm. Note that the cross-section in Figure 12 is in the same location as the one in Figure 11.

An inversion was run using WSINV3DMT, as in the synthetic borehole example with the prior/starting model as described above. A total of 6 runs, each consisting of 3 iteraions, were executed. The prior/starting model of each new run was the best fit model of the one in the run before. The results of the inversion can be seen in the lower panel in Figure 12.

### 3.3.1 Comparison between the a-priori model with previous results

The RMS of the final model where the a-priori information was used, after the 6 runs, was 2.63 whereas the RMS of the model presented in Karlsdóttir et al. (2012) was 1.74. The latter one had an initial model compiled from joint 1D inversion of TEM and MT data. The shallow structure of the two models are essentially the same and the higher frequencies are fit well in both cases (Figures 13 and 14). The deeper parts (longer periods) are, however, not as well fit in the a-priori model as the

one of Karlsdóttir et al. (2012). Reasons for this could include the different starting models and inadaquate estimation of the depth/resistivity value and thickness of the apriori deep low-resistivity structure.

Here an attempt was made to use information from seismic data in resistivity modeling by implementing known structure into the startin/prior model. The inversion seeks to retian structure it is given in the priori model and therefore the up-doming structure was hardly changed durin the inversion. This could indicate that the data are not sensitive to subtle changes in structures at depth, rather they are sensitive to larger variations.

Recommendations in the future include varying the resistivity value of the input deep low-resistivity structure and the surrounding Earth, as well as the thickness of deep the low-resistivity layer to investigate if a better fit can be reached.

**Figures:**

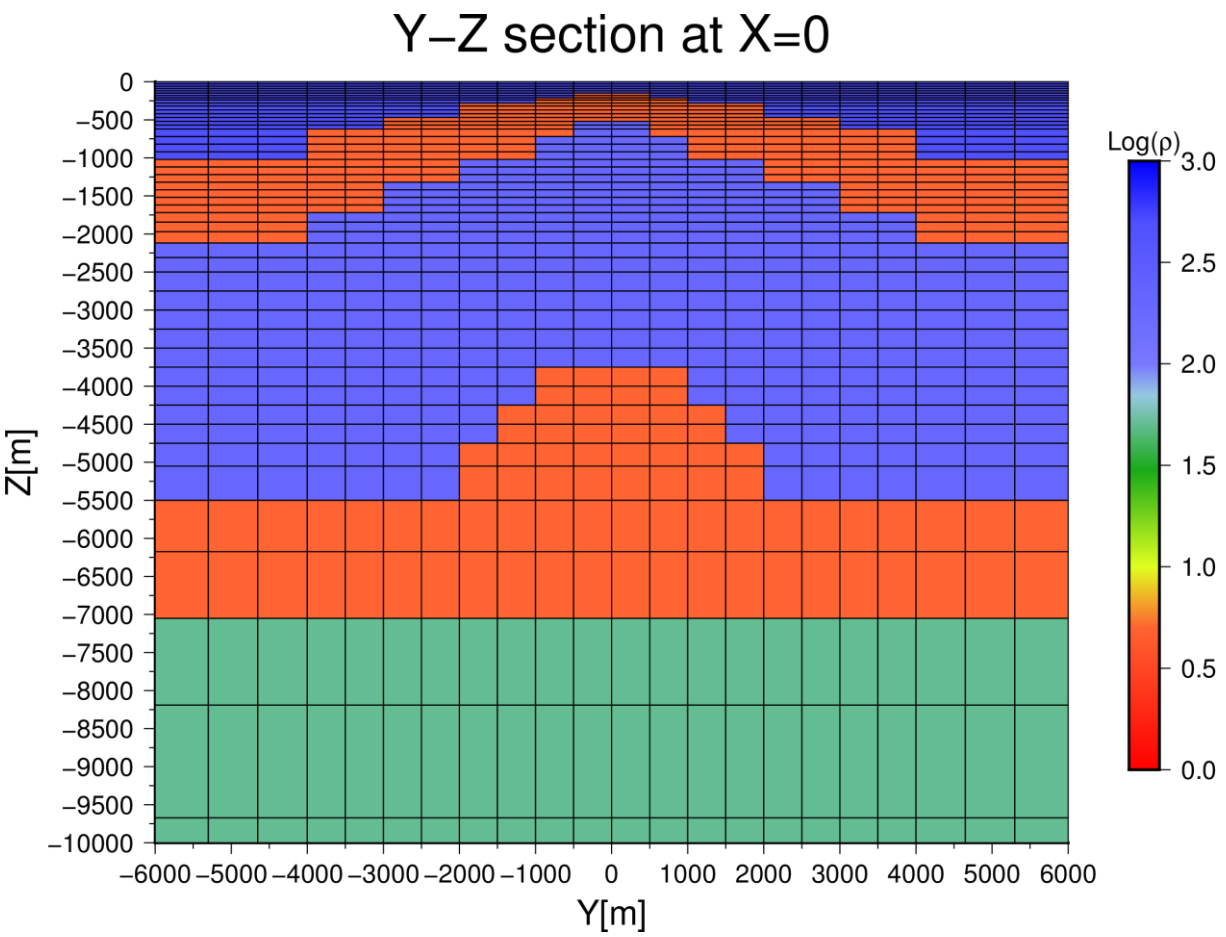


**Figure 1:** *Synthetic resistivity model immitating the resistivity structure of high-temperature geothermal systems. At the top there is a high resistive layer, then the low-resistivity cap followed by a resistive layer. Further below is a deep low-resistivity layer, as observed under most of Iceland (excluding the Reykjanes Peninsula). The deepest layer is of a medium resistivity.*

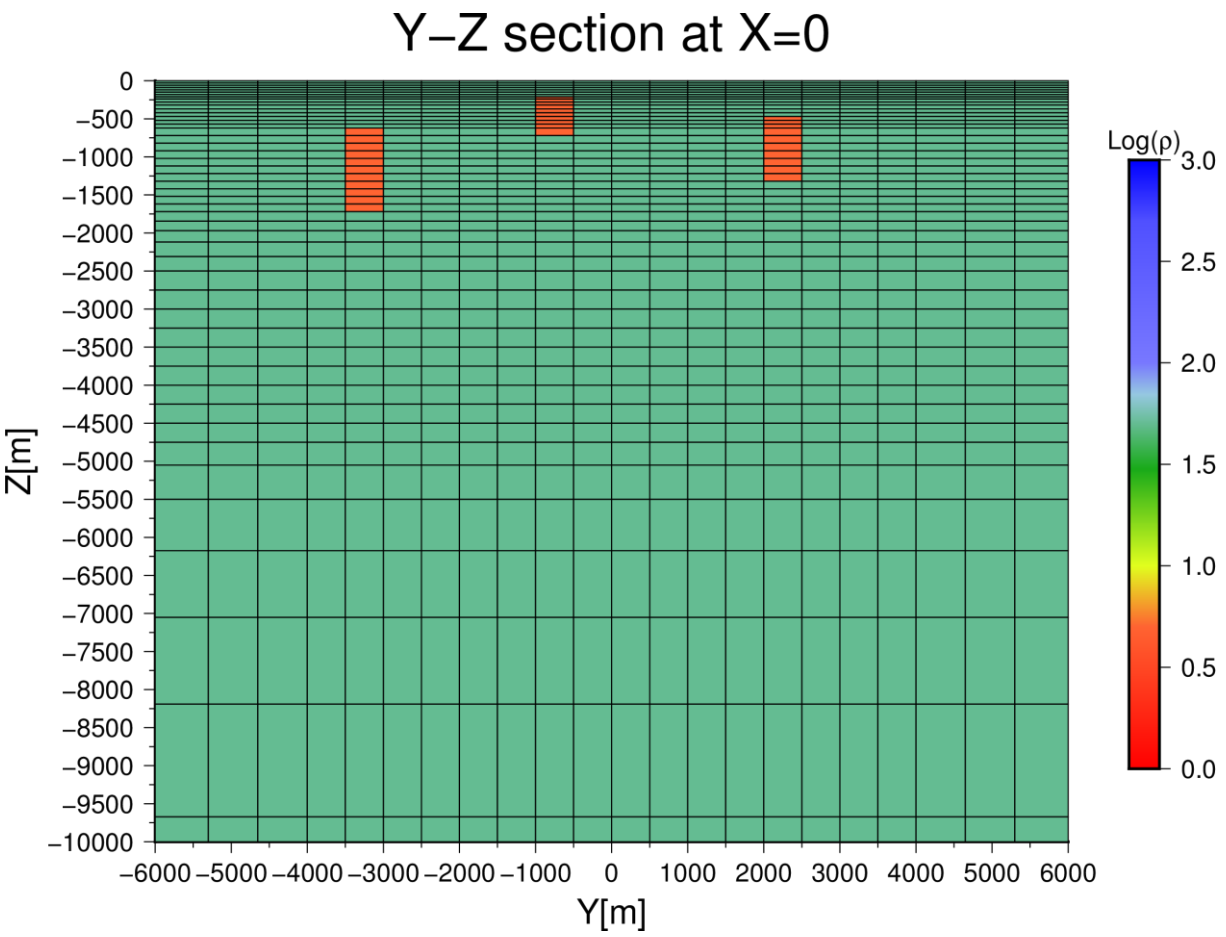


**Figure 2:** *Initial and prior model for the DISCRETE model. Three locations along the 2D high-temperature geothermal model are chosen to represent the synthetic borholes. Note that these localities are taken from the low-resistivity cap of the original model. The background matrix has a resistivity of 50 Ωm and the low-resistivity boreholes are 5 Ωm.*

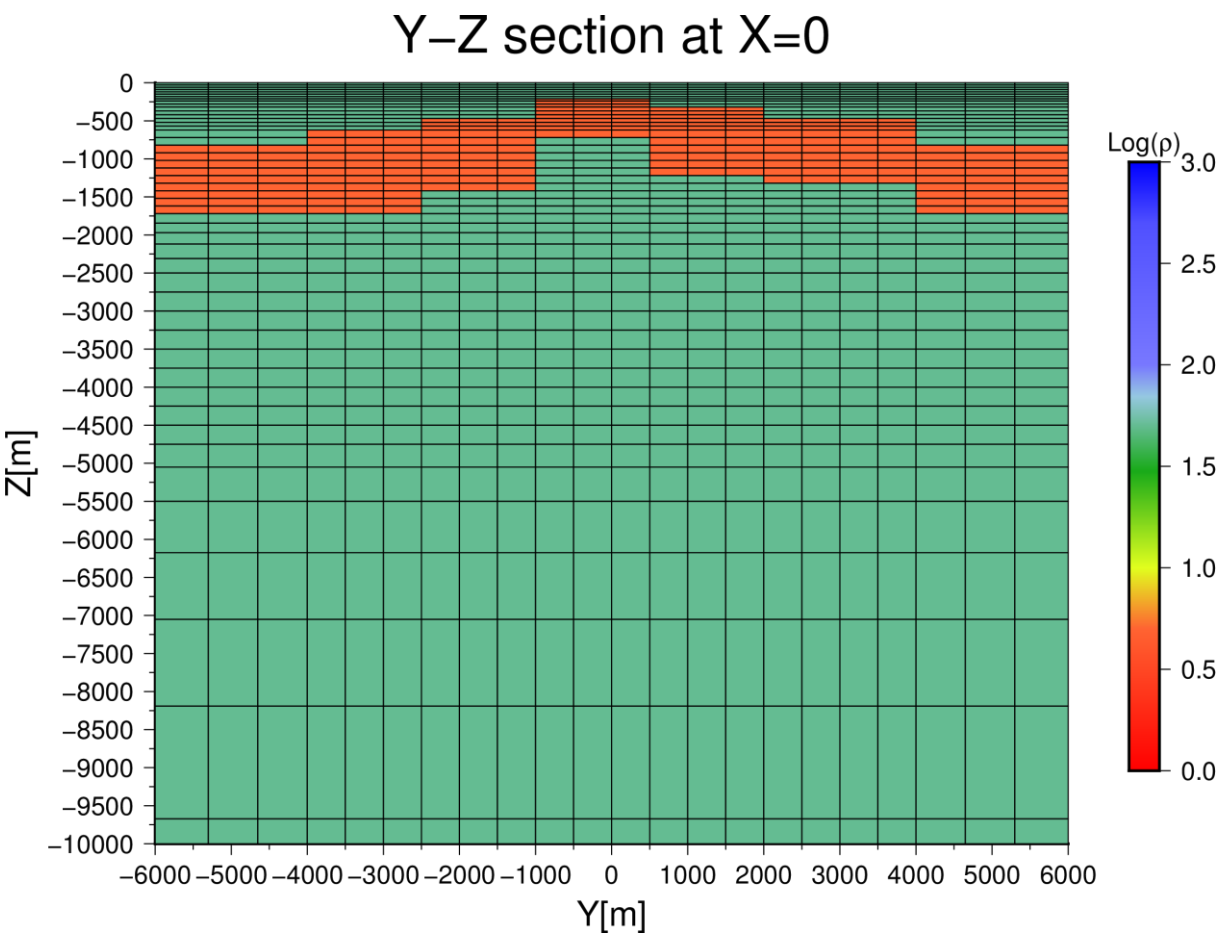


**Figure 3:** *Initial and prior model for the CONTINUOUS model. The three localities of the boreholes in the DISCRETE model are used as borehole information and a realistic continuous low-resisitivity cap is created from these information. Note that the low-resisitivity cap is not symmetric about y=0 simply because there is no information on the symmetry of the low-resistivity cap. The background matrix has a resistivity of 50 Ωm and the low-resistivity cap has a resistivity of 5 Ωm.*

Figure 4

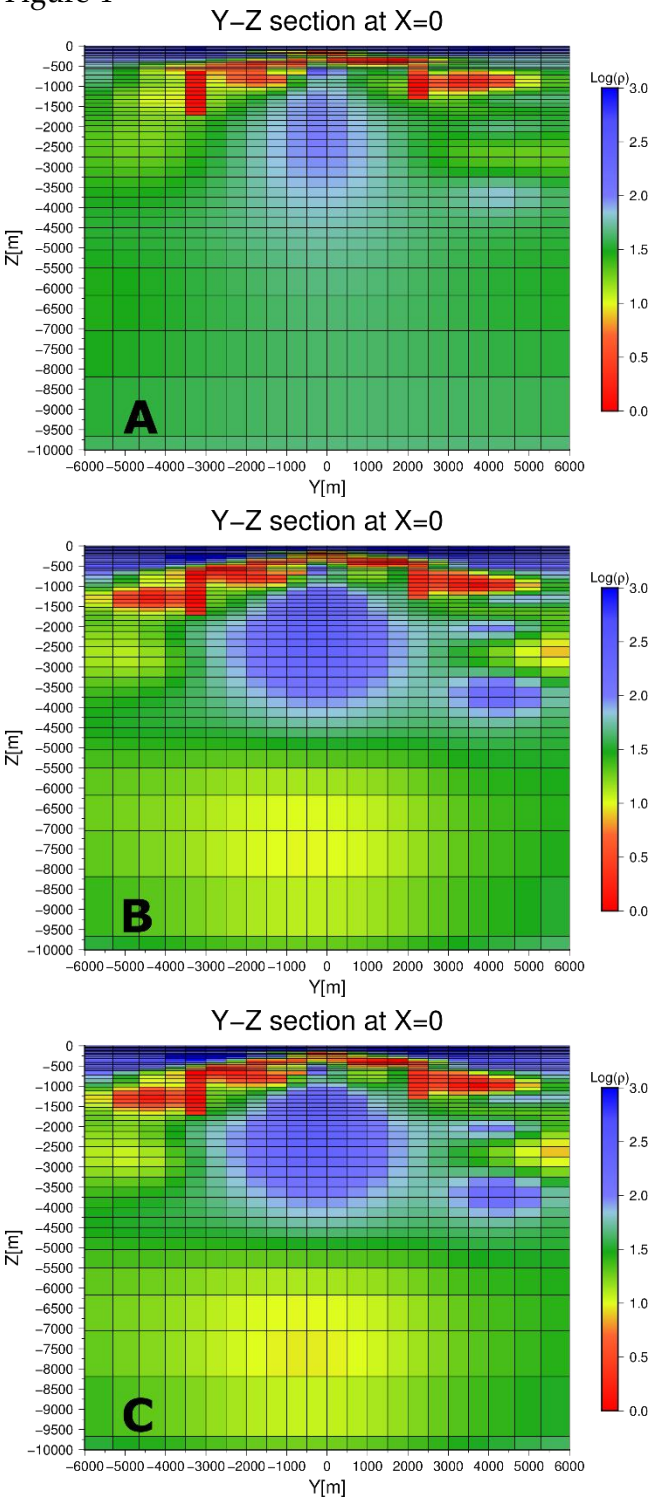


**Figure 4:** *Inversion results of the DISCRETE model showing the larger extends after the first (**A**), the second (**B**) and the third (**C**) run. The low resistivity layer is resolved as a flat layer, rather than a layer with a shape to it, as is in the input model.*

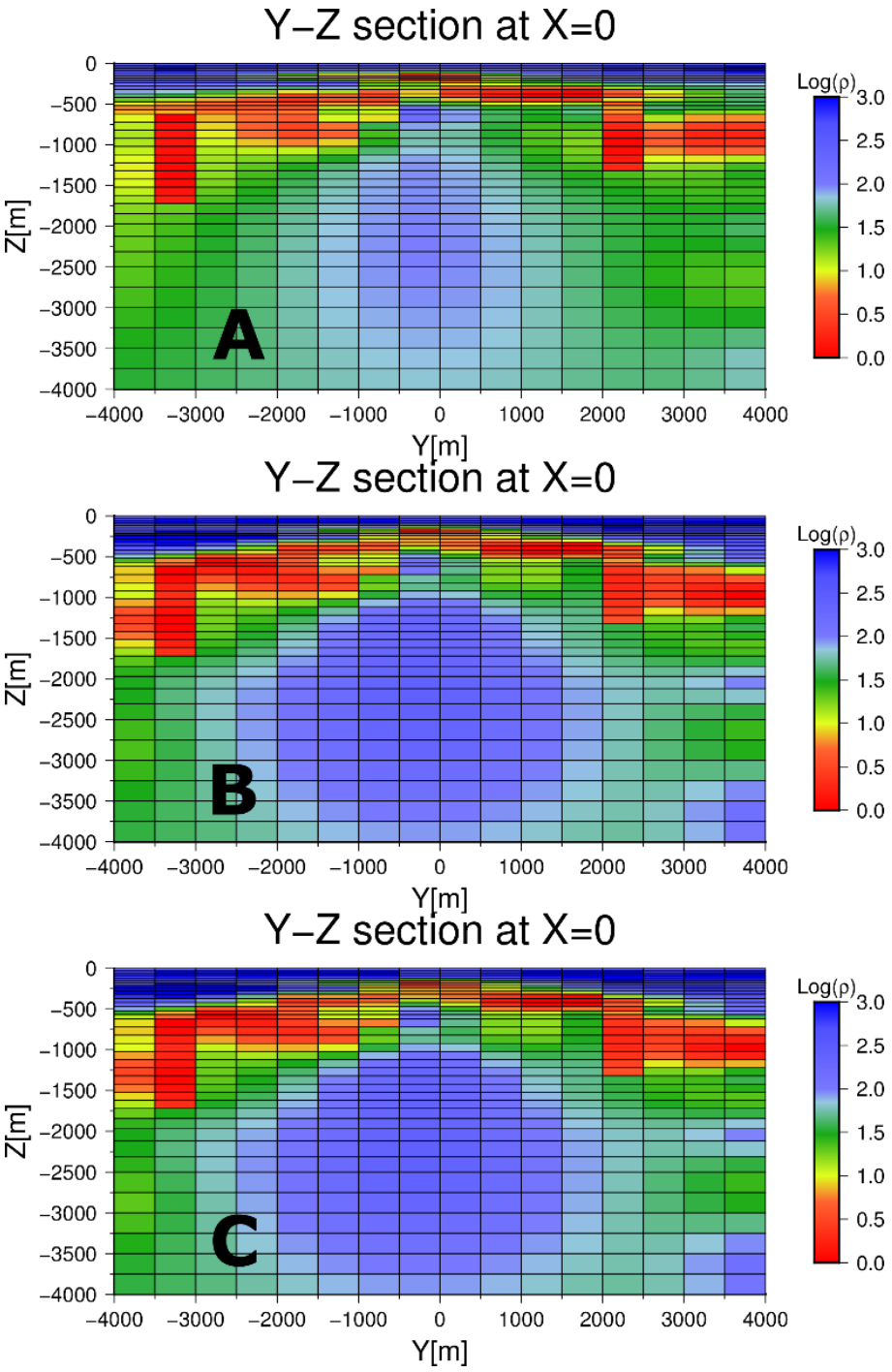


**Figure 5:** *Inversion results of the DISCRETE model showing the smaller extends after the first (**A**), the second (**B**) and the third (**C**) run.*

Figure 6

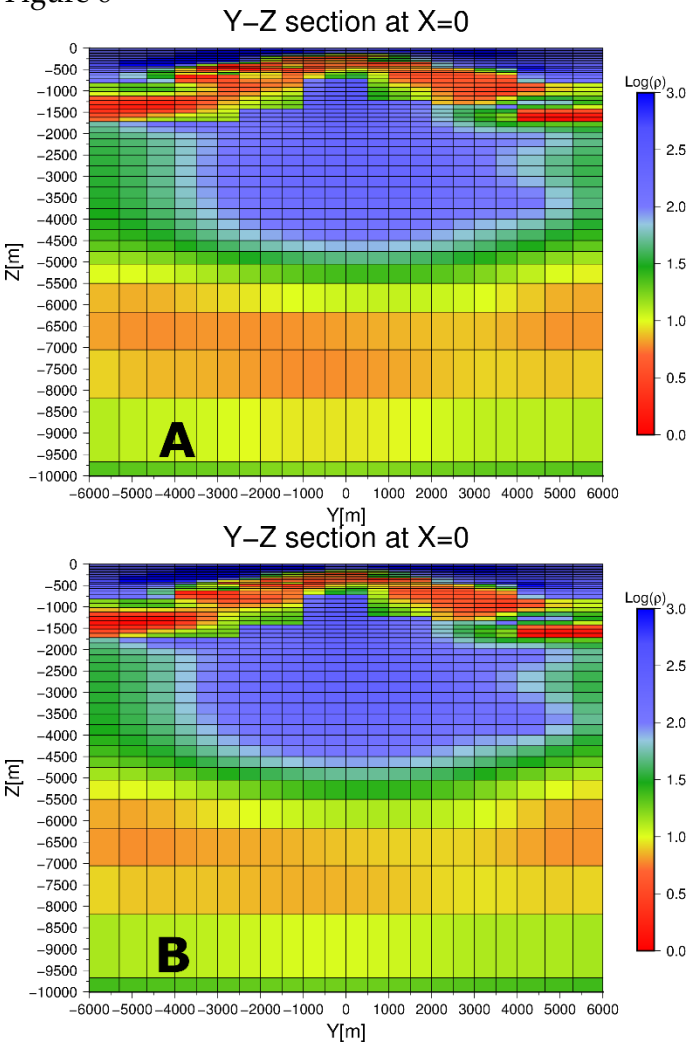


**Figure 6:** *Inversion results of the CONTINUOUS model showing the larger extends after the first (**A**) and the second (**B**) run.*

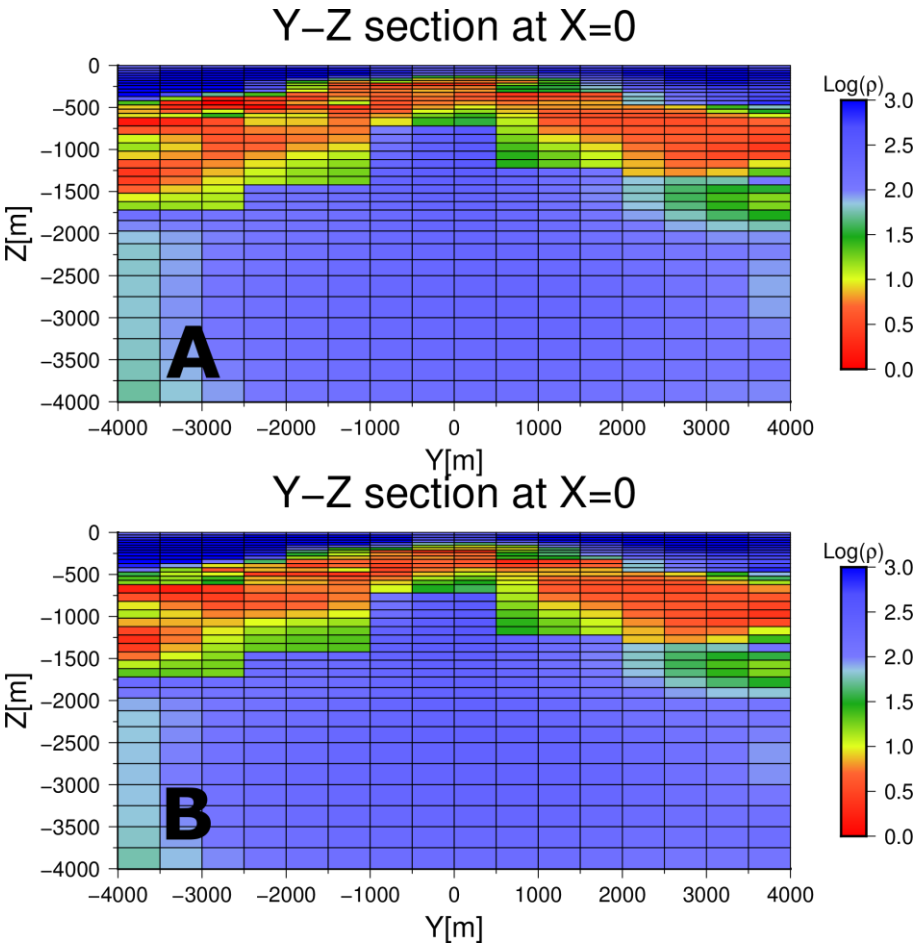


**Figure 7:** *Inversion results of the CONTINUOUS model showing the smaller extends after the first (**A**) and the second (**B**) run.*


**Figure 8:** *Map of Iceland showing the location of the Námafjall area (red bubble). Figure obtained using maps.google.com.*

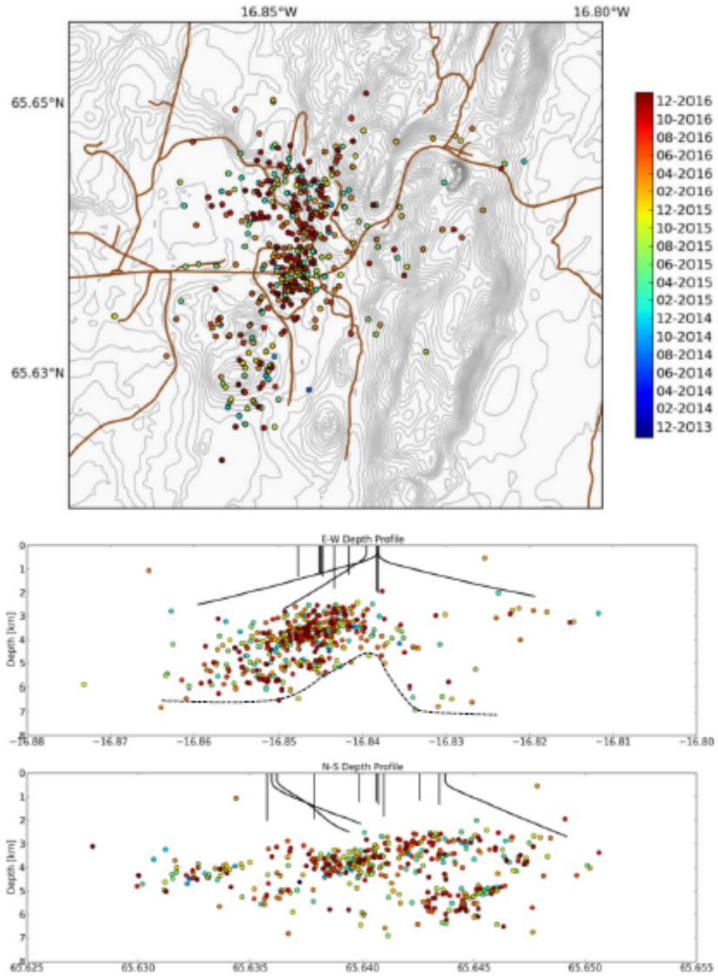


**Figure 9**: *Seismicity at Námafjall geothermal area showing an aseismic zone in the E-W cross section (middle-panel). From Ágústsson et al. (2016).*

Figure 10

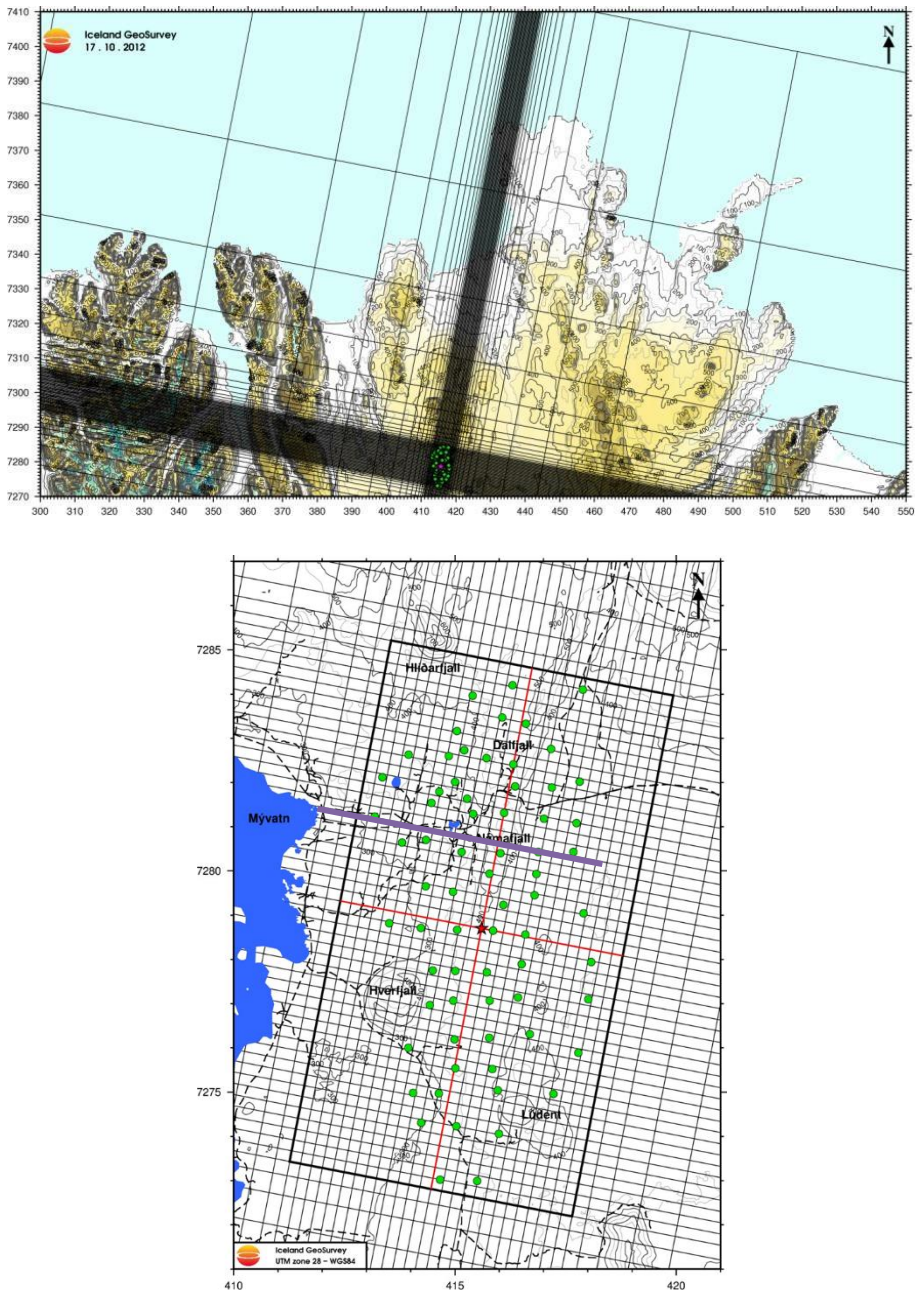


**Figure 10:** *Location and outline of the grid used for the 3D inversion. Large outline of the grid (upper panel) and the finely gridded area with a 250 m grid spacing (lower panel). The heavy black box marks the area of interest (8 x 12 km). Red star shows the origin of the grid and green dots show the MT/TEM sites used in the inversion. Yellow line indicates the location of the cross-section shown in Figure 11.*

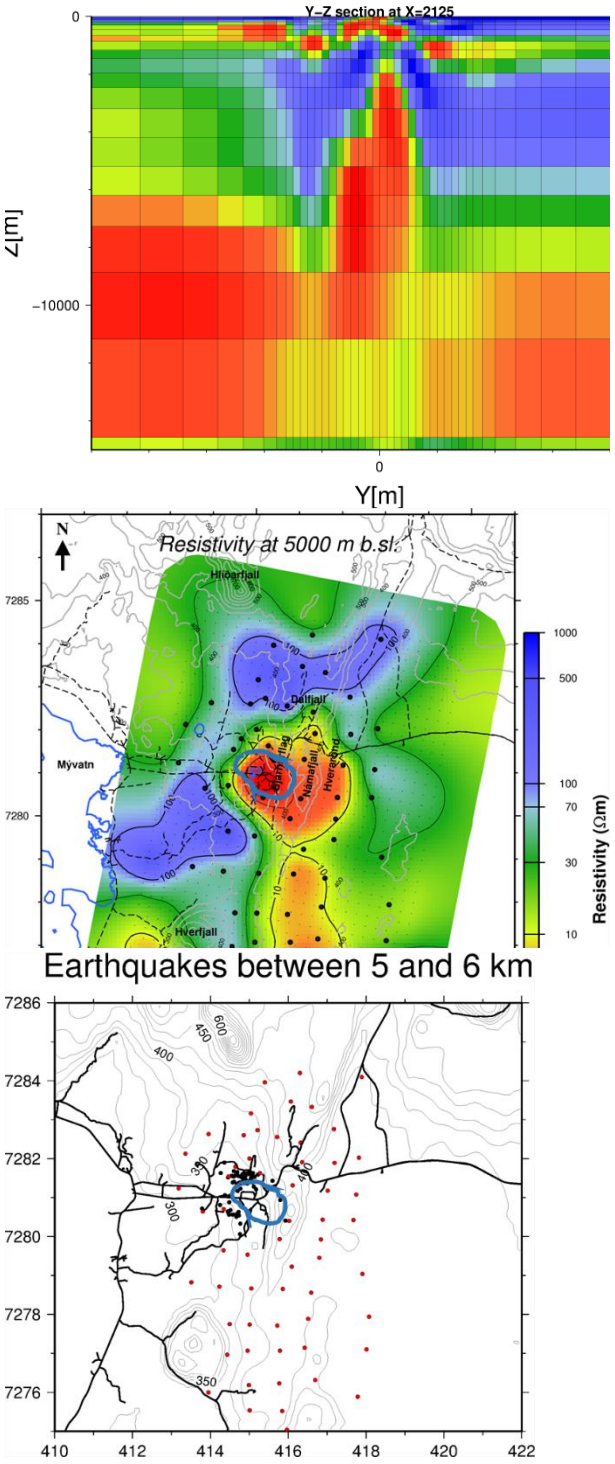


**Figure 11:** ***Top panel:*** *Cross-section through the 3D final model of Karlsdóttir et al. (2012). The location of the cross-section is shown as a yellow line in Figure 10.****Middle panel:*** *Depth-slice through the 3D resistivity model of Karlsdóttir et al. (2012) at 5000 m depth below sealevel. Blue outline shows the location of the aseismic area.* ***Bottom panel:*** *Earthquakes at 5 and 6 km depth below sea level. The red circles are seismic stations and the black cirlces are earthquakes detected between 2014 and 2016 (data from Kristjánsson et al. (2016). Blue outline as in the middle panel.*
*Figure 12*

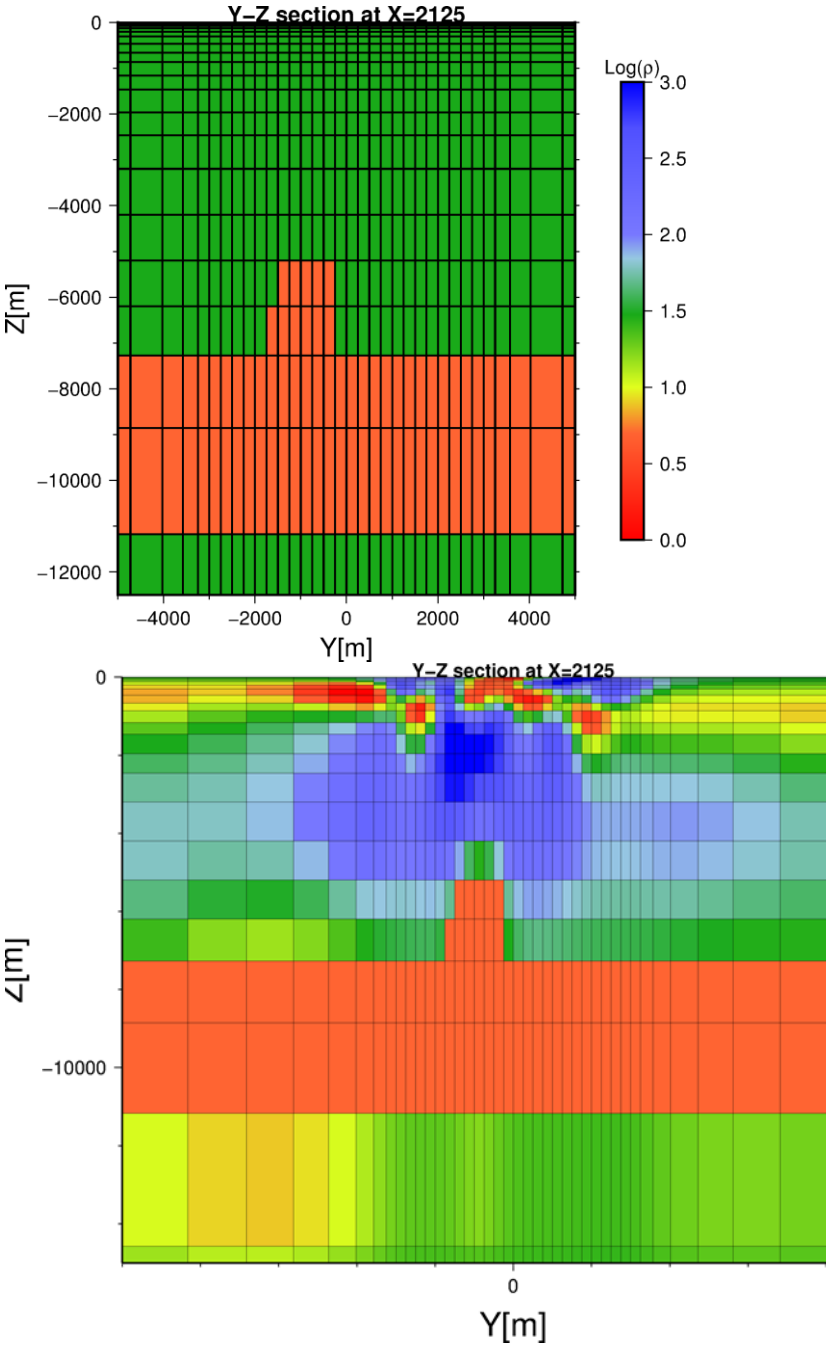


**Figure 12:** ***Upper panel.*** *The initial and prior model used to immitade the aseismic area shown in Figure 11. The low-resistivity structure has resistivity of 5 Ωm in a surrounding medium of 70 Ωm.* ***Lower panel:*** *Results of the inversion. The anomaly was not altered by the inversion. Note that these two cross-sections are in the same location as the cross-section shown in Figure 11.*

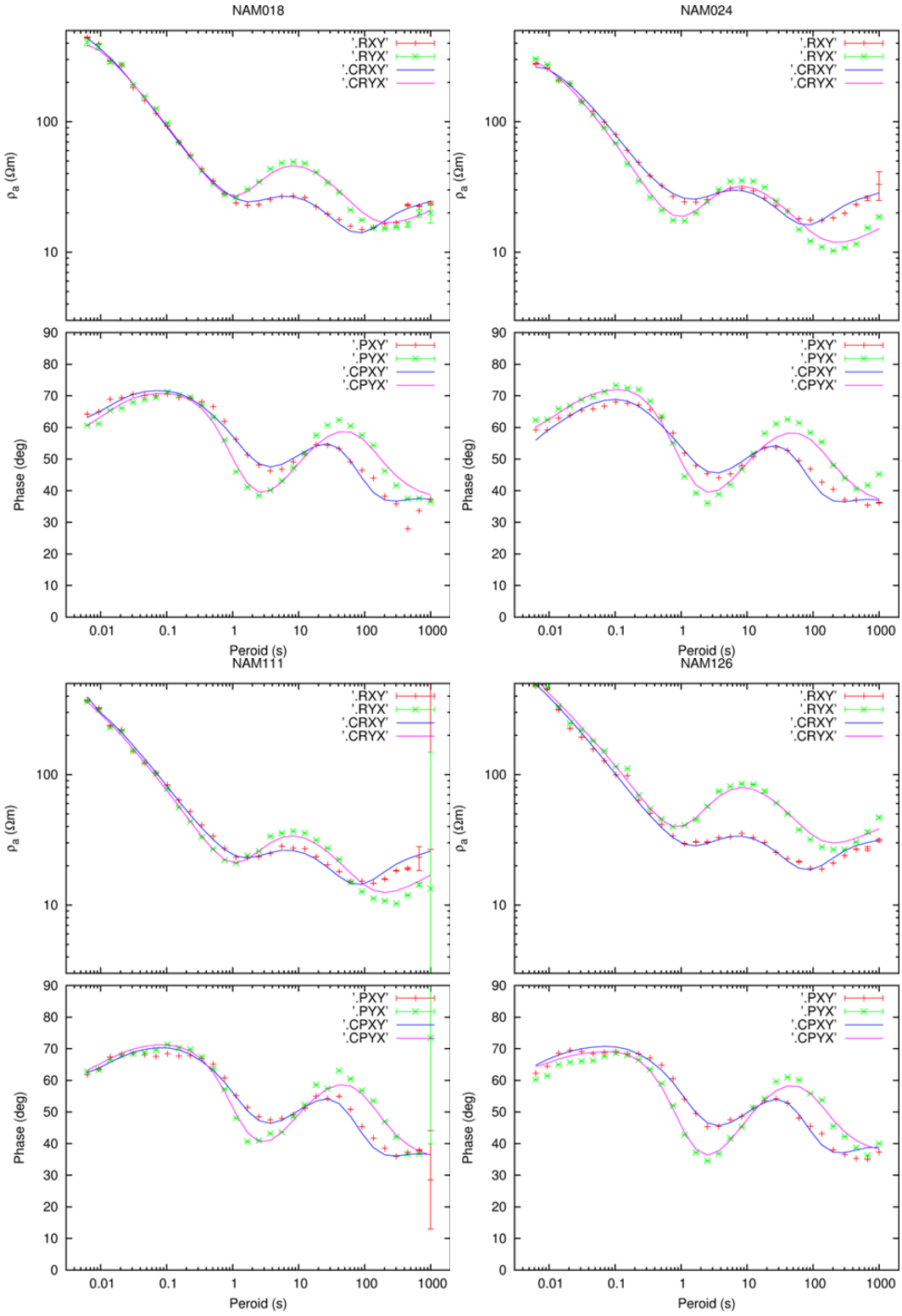


**Figure 13.** Data fit of 4 soundings (NAM018, NAM024, NAM11 and NAM126) in the model by Karlsdóttir et al. (2012). Red pluses and green crosses show the xy- and yx resistivity (data) polarizations, respectively. Blue and red lines show the model fit to the xy- and yx resistivity, respectively.

Figure 14

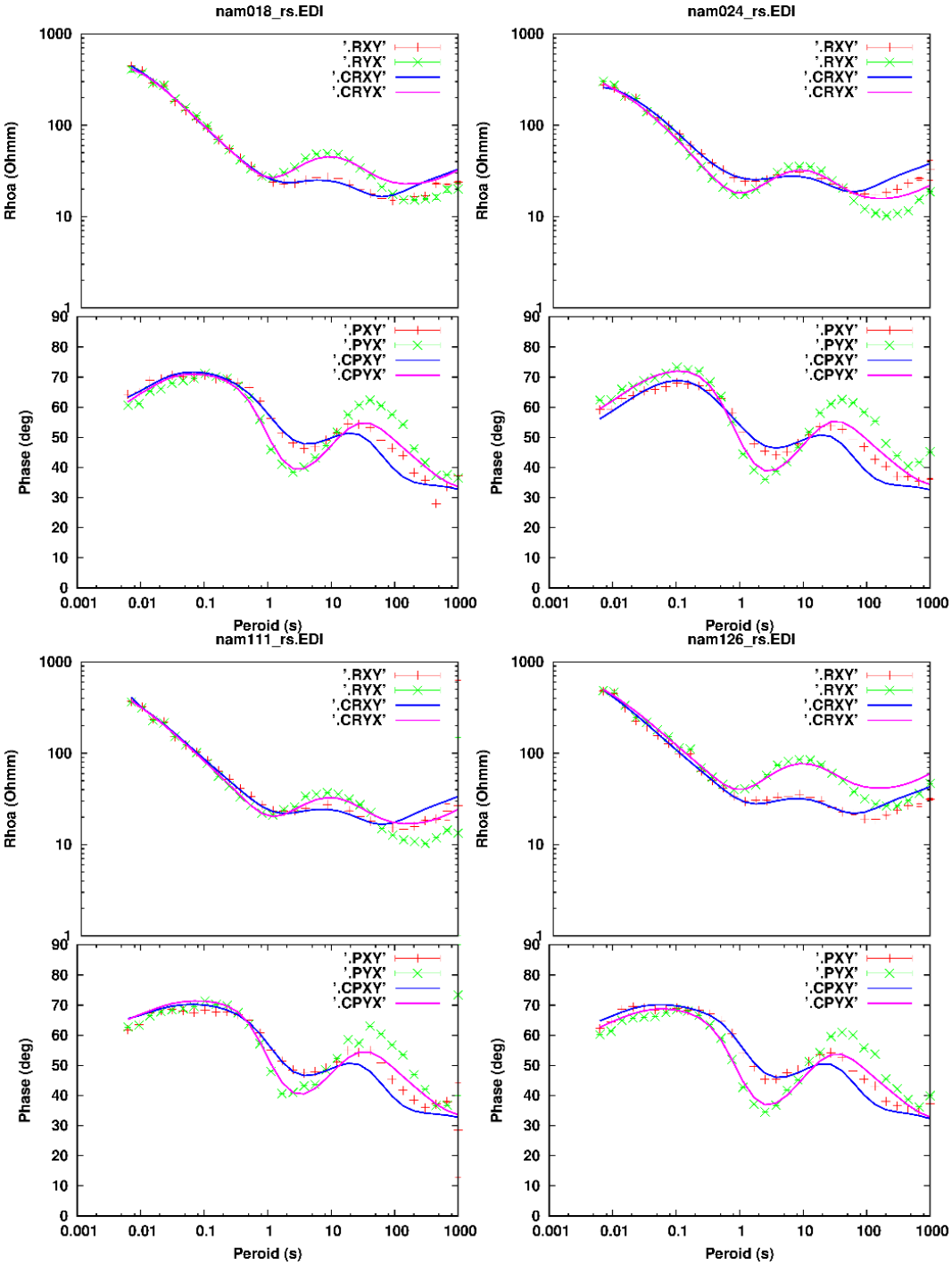


**Figure 14**. *Data fit of 4 soundings (NAM018, NAM024, NAM11 and NAM126) in the model using the a-priori information. Red pluses and green crosses show the xy- and yx resistivity (data) polarizations, respectively. Blue and red lines show the model fit to the xy- and yx resistivity, respectively*.

## 3.4 References

Árnason, K., Karlsdóttir, R., Eysteinsson, H., Flóvenz, Ó.G., Guðlaugsson, S.Th.: The resistivity structure of high-temperature geothermal systems in Iceland. *Proceedings of the WGC 2000, Japan* (2000), 923-928.

Ágústsson, K. and Guðnason, E.Á. (2016). *Jarðskjálftavirkni við Námafjall 2014 til 2016.* Iceland Geosurvey, ÍSOR-2016/085 LV-2016-128. 22p.

Karlsdóttir R., Beyene A. T. and Vilhjálmsson A. M. 2012: *Námafjall Geothermal Area Northern Iceland. 3D Inversion of MT Data.* Iceland GeoSurvey ÍSOR-2012/057 LV-2012-112. 62p.

Siripunvaraporn, W., Egbert, G., Lenbury, Y. and Uyeshima, M. (2005). *Three-dimensional magnetotelluric inversion: data-space method*. Phys. Earth Planet. Int. 150, 3–14.

Siripunvaraporn, W. and Egbert, G. (2009). *WSINV3DMT: Vertical magnetic field transfer function inversion and parallel implementation*. Phys. Earth Planet. Int. 173, 317–329.

# 4 Part three: An integrated approach to improve the reliability of the 2D inversion models

## 4.1 Introduction

The intrinsic complexity of geothermal systems and the need of an accurate integration of the geophysical parameters with the geological and hydrogeological properties of the systems still represent a challenge of the exploration geophysics. In such a scenario, we focused our research on the Larderello geothermal field (Tuscany, Italy), with the aim to explore the possibility to relate the results of electromagnetic (EM) surveys with an integrated modelling of the geothermal system.

Larderello is the oldest field under exploitation in the world. Here, the geothermal electricity production, in its modern meaning, was born. A century of industrial and scientific researches and data from hundreds of wells were not enough to understand all the geological, chemical and physical features of this complex system, and to solve the critical issues that are currently debated in the scientific community.

In addition to the acquisition of new magnetotelluric (MT) survey in a key area of the field, as described in D4.6 of the IMAGE Project, we also proposed an integrated approach to improve the reliability of the 2D inversion models, by using external information from the integrated geological modelling of the field as well as by probabilistic analysis of the MT data described in D5.3. The integrated analysis with independent datasets, such as seismic and well data, improved the knowledge on the deep structures of the Larderello field.

## 4.2 State of the art and open challenges in the EM exploration of the Larderello-Travale field

Hereby, an updated state of the art of the EM exploration activities and research projects in the Larderello field is described as well as the open challenges that the EM geophysics and the integrated modelling can contribute to solve. Since 1913, the exploration and exploitation of the Larderello field was continuously directed toward deeper levels of the systems. Magnetotellurics was therefore adopted to obtain information on the resistivity distribution at depth of the geothermal reservoir and the inferred heat sources.

Early experiments were conducted in the '70-'80s, e.g. Mosnier and Planson (1985). The authors used the "differential magnetic soundings". They observed strong conductors below the Travale area and linked this behaviour to the geothermal activity, and mentioned also the expected resistive behaviour due to the vapour state of the geothermal fluids.

Since the early '90 to the 2009, many Magnetotelluric studies have been carried out in southern Tuscany and specifically in the Larderello-Travale field in the frame of industrial exploration or in the frame of research projects. Fiordelisi et al. (1998) and Manzella (2004), obtained first indication on the deep resistivity distribution in Southern Tuscany, along very long MT profiles. The strong heterogeneity of the resistivity distribution is the main feature that all these studies highlighted, and

in particular a) the widespread low resistive responses at the depth of the exploited and dry steam reservoir and b) the low resistivity at deeper depth interpreted as due to the occurrence of melt. Why low electrical resistivity occurs in a vapour-dominated reservoir? Could the deep-buried resistivity anomalies (below the reservoirs) correspond to igneous and still melted intrusions and is it possible to image their geometries?

Further detailed magnetotelluric studies have been carried out in the Travale sector in the frame of the INTAS and I-GET European Projects during the period 2004-2009. Many MT data were acquired and multidisciplinary studies were accomplished in order to depict in details the resistivity anomalies and to understand the physics behind these electrical responses in Travale but a unique explanation was not figured out.

Manzella et al. (2006) focused on the correlation with the main active faults and the electrical resistivity distribution. In Giolito et al. (2009) and Manzella et al. (2010) the authors proposed a multidisciplinary approach that integrated the MT survey results with mineralogical analysis on cuttings and cores of the deep geothermal wells and geophysical well logs in the Travale sector. The authors excluded that mineral alteration represents the main cause of the widespread low resistivity anomaly detected by MT in the vapour-dominated reservoir, and suggested the role played by a liquid phase in the reservoir, possibly occurring in small pores, although never highlighted by production tests.

It should be mentioned that Spichak and Zakharova (2014; 2015a; 2015b) completely differed from the above described interpretations, but to the knowledge of one of the author of this report their reported temperature didn't agree with the known temperature regime of the area.

The difficulty to interpret low resistivity anomalies in dry-steam reservoirs led also a part of the scientific community to consider questionable the quality of MT data and not excluding a bias or a noise effect. The last issue was taken into account in the frame of the IMAGE Project. Coupled with the MT survey in the Lago Boracifero area described in this study, an experimental surface-hole deep ERT (Electrical Resistivity Tomography) was designed along the Venelle-2 deep geothermal well and carried out by the researchers of the CNR-IMAA (see details of the experiment design in D4.6 of Image Project). The resistivity models estimated with a controlled source DC method, show a very strong reduction of resistivity values in the metamorphic rocks in the Lago Boracifero area, confirming the MT responses in the Larderello field.

## 4.3 2D MT inversion with and without external constraints

In the frame of the IMAGE Project we have acquired a new MT survey in the Lago Boracifero sector. The survey and the resulting models were the focus of the Task 4.6 are described in D4.6. In figure 1 we show the measured MT and TDEM soundings and the profiles along which we computed the 2D inversions. Here we synthetize the main results.

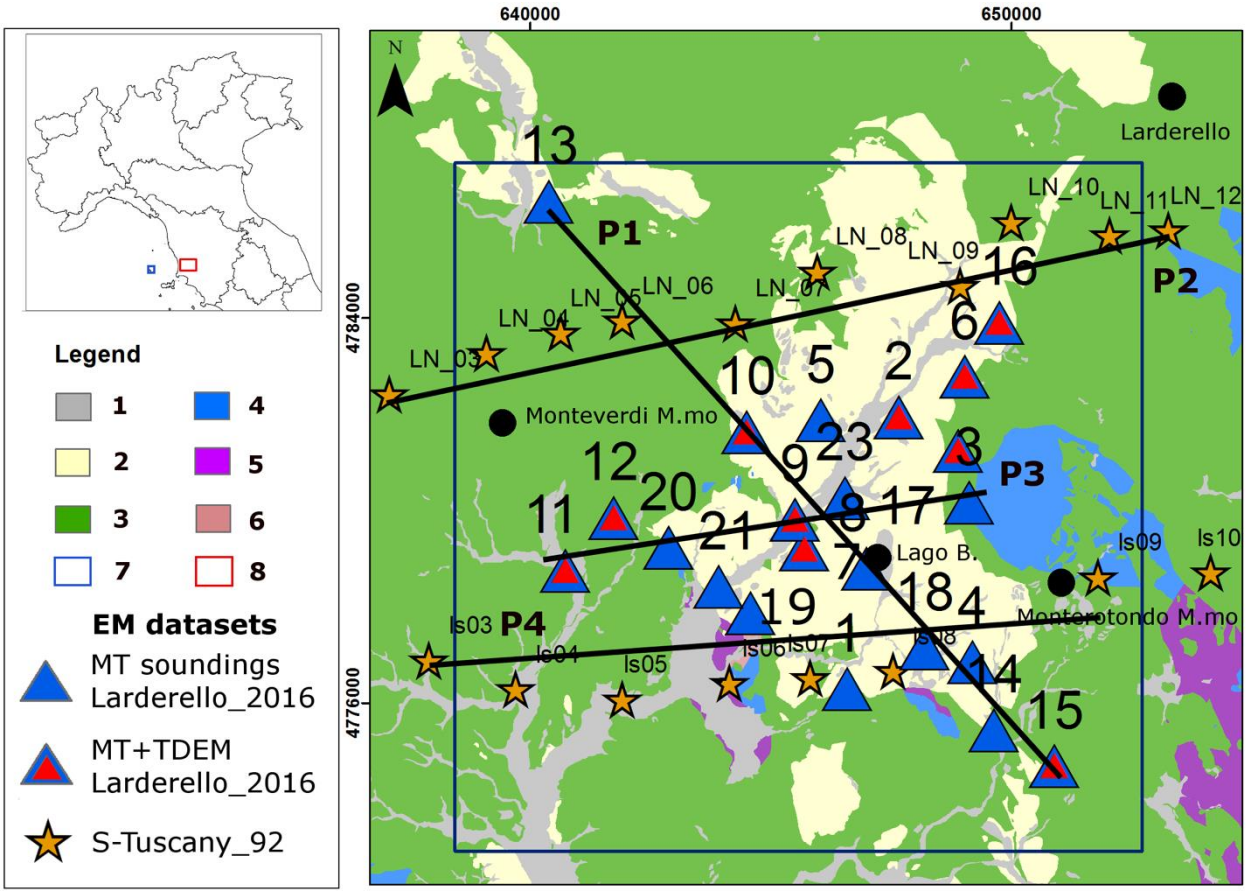


**Figure 1.** *Location of the MT soundings of old and new datasets available for the study of the Lago Boracifero area (modified from Santilano 2017): 1) Quaternary deposits; 2) Neoautochthonous terrigenous deposits (Miocene-Pliocene); 3) Ligurian and sub-Ligurian Flysch complex (Jurassic-Eocene); 4) Tuscan Nappe formations (Upper Trias-Miocene); 5) Calcare Cavernoso and anhydrites; 6) Metamorphic Units (Paleozoic); 7) Remote MT site in the Capraia Island; 8) Survey area in the Lago Boracifero sector of the Larderello field.*

For each MT profile, three resistivity models were implemented and tested as starting model for the 2D inversion:

- Homogeneous halfspace;
- Resistivity distribution by assigning resistivity values to different units of the geological model;
- interpolation of 1D resistivity distribution of PSO optimization (later PSO model).

The homogeneous a-priori model is a halfspace with a homogeneous electrical resistivity of 100 Ωm implemented on the 2D grids along the profiles.

The implementation of the a-priori models from geological information required some effort. First of all, the detailed 3D geological models for the Lago Boracifero area was built in Petrel environment. Hundreds of deep geothermal wells, seismic and geological data have been integrated and used to reconstruct the main geological surfaces Figure 2. The study of six resistivity well logs allowed the definition of resistivity values to be assigned to each geological unit.

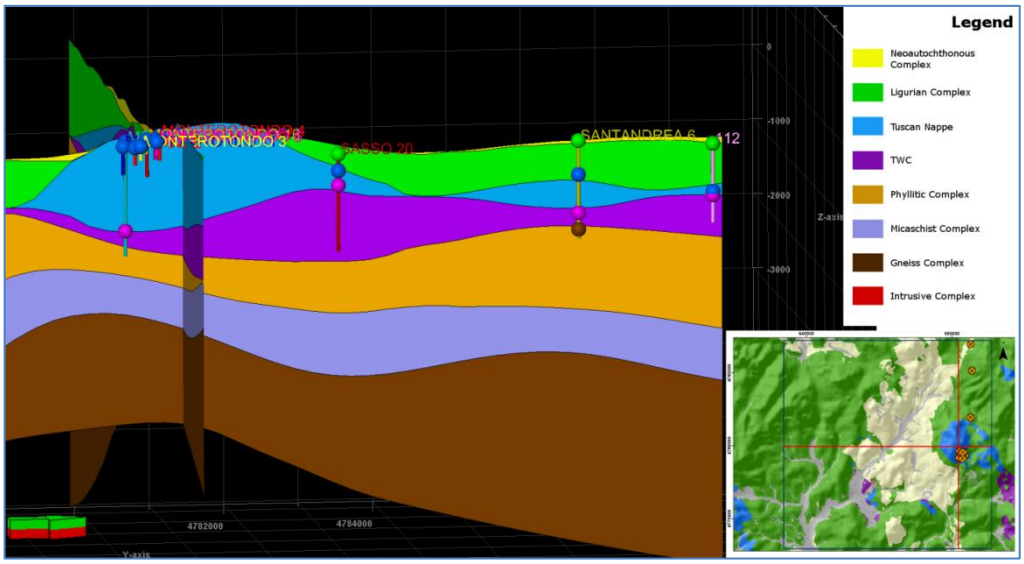


**Figure 2.** *Resulting model compared with the stratigraphic well logs (from Santilano, 2017). The location of wells and the traces of the two perpendicular profile are shown.*

As a way to constrain the inversion using only MT information we also tested the use of a-priori models based only on the MT data and not on geology. Here we applied the particle swarm optimization (PSO) to solve the 1D MT inverse problem. We interpolated the models to obtain pseudo-2D resistivity models to be used as a-priori models for the deterministic 2D inversion.
The 2D deterministic inversion was performed with the algorithm by Rodi and Mackie (2001), with different starting models used as constraints. The details on the inversion settings and the resulting models are described in D4.6.

## 4.4 Comparison among unconstrained and constrained results

The comparison among the unconstrained and constrained inversion models is a main focus of the activity in the Task 5.6. The comparison of different models along the selected profiles 1-3 is shown in figure 3.

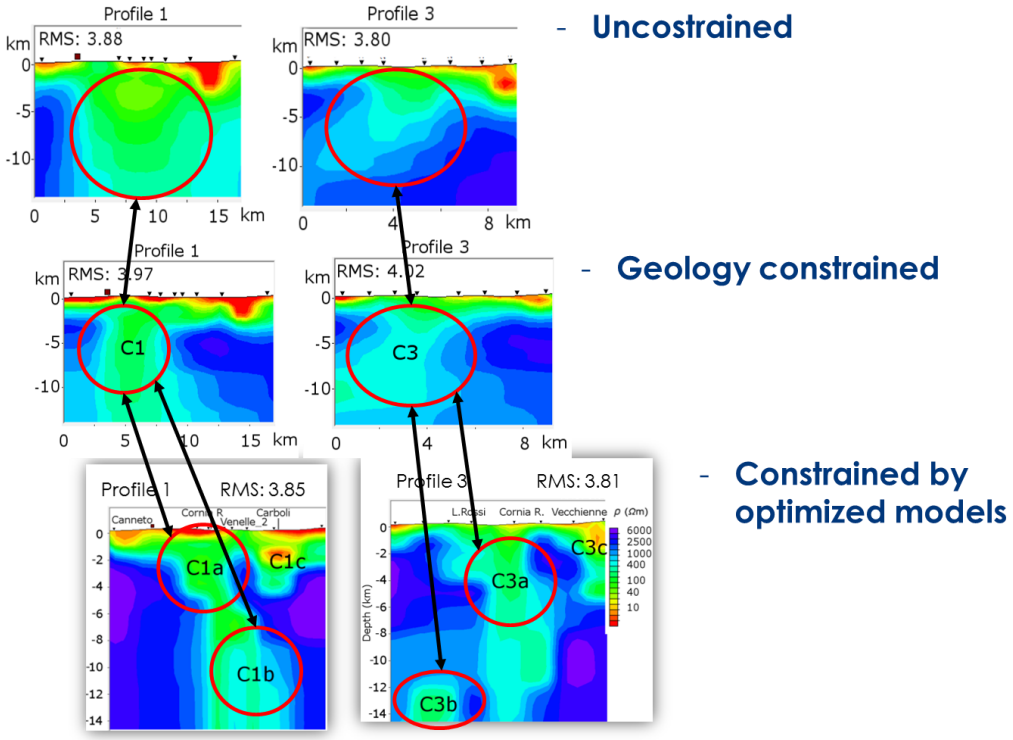


**Figure 3.** *Comparison for Profile 1 and Profile 3 of the resistivity models obtained by 2D inversion with different starting model.*

Let first analyse the results from a homogeneous half-space of 100 Ωm. The resulting models appear very smooth and lack the necessary resolution for imaging the subsurface, especially in complex structures such as in Larderello. It is clear that to fit the data a strong reduction of resistivity is required along the profiles also at depth of crystalline rocks. An important structure with a decrease of resistivity to 50-100 Ωm is highlighted, located mostly in the central part of the profiles. Some other shallow low resistivity structures coincident with Neogene basins seems to be oversized.
With regard to the use of constraints from geology, the resistivity models clearly indicate that low resistivity anomalies occur at depth of the vapour-dominated reservoir hosted in crystalline rocks and also at deeper level in spite of we constrained the inversion with deep high resistivity layers. Four main sub-horizontal layers can be recognized with the following resistivity: *1)* 3-30 Ωm, *2)* 40-200 Ωm, *3)* 2500-5000 Ωm, *4)* 100-400 Ωm. As expected, the low resistivity shallow layer, with values in the range of 3-30 Ωm, corresponds to the Neoautochthonous and Ligurian Complexes.

The underlying layer, characterized by resistivity values in the range of 40-200 Ωm, is located at a structural level coincident with the Tuscan Complex, Tectonic Wedge Complex (TWC) and most of the Phyllitic Complex.

The third layer, characterized by resistivity values in the range of 2500-5000 Ωm, corresponds mainly to the Micaschist, Gneiss and Intrusive complexes.

Finally, at depth higher than 7 km, a general decrease of resistivity is observed with values locally lower than 400 Ωm.
All the MT profiles in the *Lago Boracifero* sector show a very important sub-vertical structure cross-cutting the main sub-horizontal layers previously described and characterized by low resistivity,

with average values of about 150 Ωm. The use of constraints from geology seem to increase the resolution, as pointed out by an additional analysis with other geological and geophysical data despite the RMS are similar or slight higher than the unconstrained.

With regard to the inversions constrained from PSO optimized models, the complex subsurface structure of the Larderello system appears much more detailed than in any other inversion result. As for any model inversion, the PSO constrained inversion models image low resistivity anomalies in the central sector of the profile. In this case, however, the resolution appears even better than that of geologically-constrained inversions (C1 and C3), so that the anomalies differentiate into C1a-b and C3a-b. The results are quite consistent in terms of RMS, which are lower than the corresponding ones obtained from geologically constrained inversions.

## 4.5 Discussion on the impact on the conceptual model of the Lago Boracifero sector

The aim of this work was to improve the knowledge on the deep structures of the Lago Boracifero sector (Larderello field) being of interest firstly for its geological complexity and also for the possibility to explore deep-seated unconventional geothermal resources. The results from homogeneous a-priori models appear very smooth and lack the necessary resolution for imaging the subsurface. The adoption of the 3D geological model and geophysical well logs for constraining the 2D inversion allowed the increase in resolution to image the deep structure of the Larderello-field.

In the Lago Boracifero sector, the upper units are very conductive due to lithology of the Neoautochthonous and Ligurian Complexes. Their corresponding resistivity values resulting from inversion was in the range of 3-30 Ωm, in perfect agreement with the resistivity well logs.

The intermediate structural levels (up to 2500 m b.g.l.) coincident mainly with the TWC and most of the Phyllitic Complex are characterized by resistivity values in the range of 40-200 Ωm (mostly 100 Ωm). These values are far from the corresponding resistivity measured by DLL/IL well logs of the Travale area. It is possible, in our opinion, that the widespread low resistivity of Phyllites is due to the presence of interbedded layers of graphite. Along the well log data, these layers can be recognized as thin and very conductive layers alternated to extremely resistive ones. Instead, being the magnetotellurics a diffusive method, it provides averaged resistivity values over very large volumes. As mentioned previously, a recent experimental surface-hole deep ERT (along the Venelle-2), yet unpublished, confirmed a very strong reduction of resistivity values in these metamorphic rocks.

On the other hand, in the Lago Boracifero area the Micaschist, Gneiss and Intrusive rocks are characterized by high resistivity values in the range of 2500-5000 Ωm as expected by resistivity well log value.
Large low resistivity anomalies, with values of about 150 Ωm, locally interrupt the resistive metamorphic units. These anomalies appear sub-vertical in the 4 profiles, Profile 1 to Profile 4, and seem related to a structure elongated N30E. The decrease of resistivity in the Micaschist, Gneiss and

Intrusive complexes would suggest a strong influence of the hydrothermal circulation. This interpretation can imply two main processes: i) the occurrence of a minor contribution of liquid-phase in the vapour dominated reservoir (hypothesis not confirmed by well tests) and/or ii) the effect of more or less pervasive hydrothermal alteration, possibly a remnant of the effect of an old, liquid phase fluid circulation.

At mid-crustal level, below 6 km depth, a further reduction of resistivity is recognized in all the MT Profiles in the Lago Boracifero area. These anomalies can be ascribed to the partially melted granitic intrusions that act as heat source of the field. Considering this assumption, the heterogeneous distribution of resistivity at this depth can be in part explained as different percentage of melting in the rock volume.

Another important aspect that can be pointed out from the MT modelling is the role of faults in controlling the hydrothermal circulation of the Larderello field. This is not trivial considering that even detailed 3D reflection seismic results and decades of exploration did not led to a commonly accepted structural model.

The results drove us to identify the main geological structures that in our opinion could strongly control the evolution of the geothermal area of Lago Boracifero.

We particularly refer to the Cornia Fault that is imaged as a wide sub-vertical low resistivity structure located along the homonymous river. The MT results led us to interpret this structure as a fault that controlled the magmatic activity in this specific sector and possibly controls the hydrothermal circulation, along a very wide (some kilometres) shear zone oriented N30E.

## 4.6 Correlation with seismic models

In figure 4 we summarize one of the main result of this activity, i.e. the Cornia Fault imaged by the MT profiles (constrained with PSO models) and its correlation with seismic studies in the area.
The P-wave anomaly, as derived from 3D tomography of local earthquakes (Batini et al., 1995), is showed for values lower than 5000 m/s. The authors related the reduction of P-wave velocity to the occurrence of an intrusive still partial melted body. The CROP18 (reflection) seismic profile (Brogi et al., 2005) is overlapped on the MT Profile 1 since the traces coincide. The correspondence of mid-crustal electrical resistivity anomaly with the low seismic velocity body is striking in both cases.

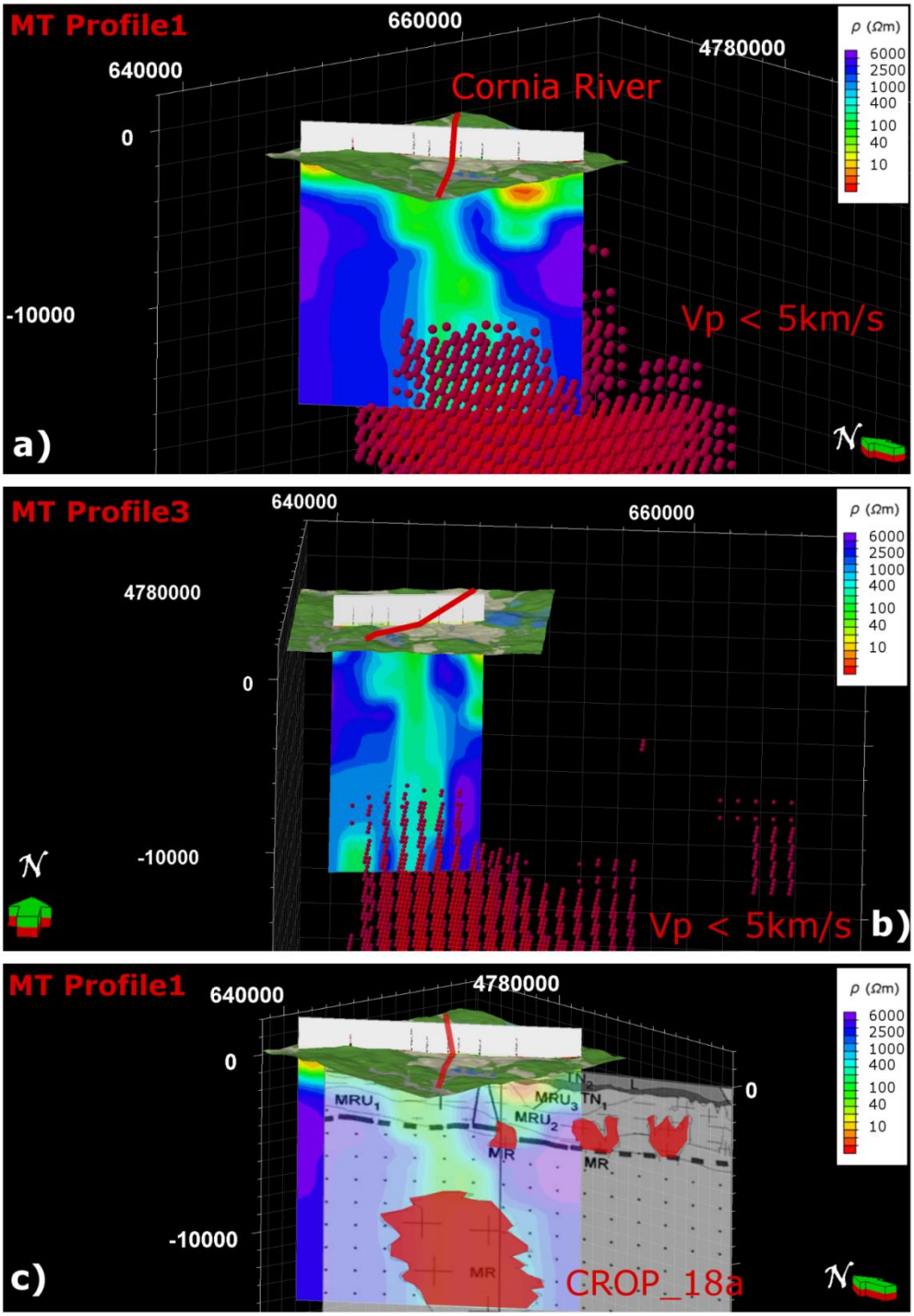


**Figure 4.** *MT Profile 1 plotted in 3D and compared with other geophysical data (from Santilano, 2017): Comparison between the MT Profile 1 (a) and Profile 3 (b) and the anomaly of seismic low velocity (Batini et al., 1995) here filtered for the values below 5 km/s; b) MT plotted in 3D with the geological map; c) comparison between the Profile1 and the deep seismic profile CROP 18a (Brogi et al., 2005), particularly the intrusive rocks (MR) imaged by the seismic reflection data are highlighted in red.*

A control of the sub-vertical structure (i.e. Cornia Fault) in favouring (as regional mechanical discontinuity) the emplacement of intrusive bodies in this area, can be supposed. The resistivity

model in the other MT profiles, particularly in Profile 4 (toward Larderello), show a wider low resistivity anomaly, in terms of spatial extension, at mid-crust depth. This aspect seems in accordance with seismological studies. Particularly interesting is the clear correspondence of the Low Velocity Zone (LVZ) resulting from the inversion of teleseismic travel time residuals (Foley et al., 1992).

## 4.7 Conclusions and recommendations

In this report we proposed an integrated approach that greatly improved the knowledge on the deep structures of the system on the basis of the critical review of deep well data, geological and geophysical data and the analysis of new and previously acquired MT data in the Larderello-Travale field.

We achieved the resistivity models by 2D deterministic inversion. We focused on the understanding of the reliability of the a-priori model for the inversion procedure. For this reason we implemented and tested three sets of starting models: i) homogeneous (without external constraints), ii) geological (from the integrated model) and iii) interpolation of 1D models.

The resulting models constrained with detailed and accurate geological information as well as using 1D models showed higher resolution than those unconstrained (i.e. from homogeneous half-space). We demonstrated how the a-priori information from the analysis of MT data, i.e. by PSO optimization in our case, greatly improved the inversion results even those geologically constrained. This is not a trivial issue for the exploration of geothermal greenfield, lacking of underground data.

## 4.8 References

Batini, F., Fiordelisi, A., Graziano, F., Toksöz, M.N. (1995). Earthquake Tomography in the Larderello Geothermal Area, in: Proceedings of the World Geothermal Congress, 1995-2, 817-820.

Brogi, A., Lazzarotto A., Liotta, D., Ranalli, G., CROP18 Working Group (2005). Crustal structures in the geothermal areas of southern Tuscany (Italy): Insights from the CROP 18 deep seismic reflection lines. Journal of Volcanology and Geothermal Research, 148, 60– 80.

Fiordelisi, A., Mackie, R., Manzella, A. Zaja, A. (1998). Electrical features of deep structures in Southern Tuscany (Italy). Annals of Geophysics, 41(3), 333-341.

Foley, J.E., Toksoz, M.N., Batini, F. (1992). Inversion of teleseismic traveltime residuals for velocity structure in the Larderello geothermal system, Italy. Geophys. Res. Letters, 19, 5-8.

Giolito, C., Ruggieri, G., Manzella, A. (2009). The relationship between resistivity and mineralogy at Travale, Italy. GRC Transaction, vol 33, 2009

Manzella, A. (2004). Resistivity and heterogeneity of Earth crust in an active tectonic region, Southern Tuscany (Italy). Annals of Geophysics, 47(1), 107-118.

Manzella, A., Spichak, V., Pushkarev, P., Sileva, D., Oskooi, B., Ruggieri, G., Sizov, Y. (2006). Deep fluid circulation in the Travale geothermal area and its relation with tectonic structure investigated by a magnetotelluric survey. In Proceedings, Thirty-First Workshop on Geothermal Reservoir Engineering Stanford University, Stanford, California.

Manzella, A., Spichak, V., Pushkarev, P., Sileva, D., Oskooi, B., Ruggieri, G., Sizov, Y. (2006). Deep fluid circulation in the Travale geothermal area and its relation with tectonic structure investigated by a magnetotelluric survey. In Proceedings, Thirty-First Workshop on Geothermal Reservoir Engineering Stanford University, Stanford, California.

Mosnier, J. and Planson, F. (1985). Differential magnetic soundings in the Travale geothermal area. Geothermics, 14, 5/6, 749-754.

Rodi, W. and R.L. Mackie, 2001. Nonlinear conjugate gradients algorithm for 2-D magnetotelluric inversion: Geophysics, 66 no. 1, P174-P187, doi: 10.1190/1.1444893

Santilano, A., 2017. Deep geothermal exploration by means of electromagnetic methods: New insights from the Larderello geothermal field (Italy). Doctoral dissertation, Politecnico di Torino

Spichak V.V. and Manzella, A. (2009). Electromagnetic sounding of geothermal zones. Journal of Applied Geophysics, 68, 459-478. doi:10.1016/j.jappgeo.2008.05.007.

Spichak, V.V. and Popova, I.V. (2000). Artificial neural network inversion of MT data in terms of 3D earth macro-parameters. Geophysical Journal International, 42, 15-26.

Spichak, V.V. and Zakharova, O.K. (2014). Gaseous vs aqueous fluids: Travale (Italy) case study using EM geothermometry. Proceeding of 39th Workshop on Geothermal Reservoir Engineering, Stanford University, USA.